THE UNIVERSITY OF ALBERTA

MONITORING CONTAMINANT PLUMES IN GROUNDWATER USING A THREE-DIMENSIONAL GRID OF ELECTRODES

by

Bruce G. Bennett

A THESIS

SUBMITTED TO THE FACULTY OF GRADUATE STUDIES AND RESEARCH

IN PARTIAL FULFILMENT OF THE REQUIREMENTS FOR THE DEGREE

OF MASTER OF SCIENCE

DEPARTMENT OF GEOLOGY

EDMONTON, ALBERTA

SPRING, 1989

Permission has been granted to the National Library of Canada to microfilm this thesis and to lend or sell copies of the film.

The author (copyright owner) has reserved other publication rights, and neither the thesis nor extensive extracts from it may be printed or otherwise reproduced without his/her written permission.

L'autorisation a été accordée à la Bibliothèque nationale du Canada de microfilmer cette thèse et de prêter ou de vendre des exemplaires du film.

L'auteur (titulaire du droit d'auteur) se réserve les autres droits de publication; ni la thèse ni de longs extraits de celle-ci ne doivent être imprimés ou autrement reproduits sans son autorisation écrite.

ISBN 0-315-52987-3

THE UNIVERSITY OF ALBERTA

RELEASE FORM

NAME OF AUTHOR: BRUCE GEORGE BENNETT

TITLE OF THESIS: MONITORING CONTAMINANT PLUMES IN GROUNDWATER USING A THREE-DIMENSIONAL GRID OF ELECTRODES

DEGREE: MASTER OF SCIENCE

YEAR THIS DEGREE GRANTED: SPRING, 1989

Permission is hereby granted to the UNIVERSITY OF ALBERTA LIBRARY to reproduce single copies of this thesis and to lend or sell such copies for private, scholarly or scientific research purposes only.

The author reserves other publication rights, and neither the thesis nor extensive extracts from it may be printed or otherwise reproduced without the author's written permission.

B.G. Bennett

31 Kevin Drive
Fonthill, Ontario
L0S 1E0

Date: December 8, 1988

THE UNIVERSITY OF ALBERTA

FACULTY OF GRADUATE STUDIES AND RESEARCH

The undersigned certify that they have read, and recommend to the Faculty of Graduate Studies and Research for acceptance, a thesis entitled MONITORING CONTAMINANT PLUMES IN GROUNDWATER USING A THREE-DIMENSIONAL GRID OF ELECTRODES submitted by Bruce George Bennett in partial fulfilment of the requirements for the degree of MASTER OF SCIENCE.

Frank W. Schwartz
(Supervisor)

Date: Nov 28, 1988

ABSTRACT

A new electrical method for monitoring contaminant plumes in groundwater is presented. The technique involves the use of a three-dimensional grid of electrodes installed in the ground. Current is introduced through any pair of electrodes with voltage recorded between the two intermediate electrodes. Using all possible combinations of electrodes, this operation is repeated in both a downhole and crosshole manner, thereby scanning the entire region covered by the grid. By assembling all of the voltage measurements, an apparent conductivity distribution of the subsurface is produced using a simple analytical equation.

In the absence of field data, the method was evaluated theoretically with the use of a numerical model. Results from a sensitivity analysis indicate that crosshole and downhole scans can be used in combination with each other to infer the location of a plume based on the conductivity pattern provided by each one. Crosshole scans are not particularly useful in resolving the vertical position of a plume, but rath[illegible]its horizontal location. For this to occur, however, the horizontal extent of a plume must be roughly equal to, or exceed, the horizontal spacing between boreholes. Downhole scans can more accurately determine the vertical position of a plume, limit its probably horizontal extent and, because of its smaller "a" spacing, provide a closer estimate of the actual conductivity. A downhole scan, however, must pass through a portion of the plume to obtain results which could be considered as significant.

Simulated background noise created by heterogeneities in the medium, were eliminated from the conductivity pattern by employing the concept of residual mapping. Normalizing the data with a proper set of background conditions serves to highlight any variation in conductivity which could arise from the introduction of a plume in the subsurface.

By introducing current and measuring voltages within the ground, this technique provides for a more focused and systematic investigation of the subsurface. This also avoids the loss of information with depth which inevitably accompanies a conventional surface method. It is suggested that the borehole electrode network could assume the role of providing low-cost detection duties for a site, in combination with chemical data given by wells.

ACKNOWLEDGEMENTS

I would like to offer a special thanks to my supervisor, Dr. F. W. Schwartz, for his interest and financial support throughout this project. This insight, thoughtful suggestions and constructive review of the thesis are gratefully acknowledged. The helpful comments made by the members of my examining committee, Dr. R. A. Burwash, Dr. K. Muehlenbachs and Dr. J. D. Scott are also sincerely appreciated. In particular, I would like to thank Dr. D. Hackbarth for originally suggesting the topic of this thesis and for the confidence he placed in me towards completing it.

I also benefited from the invaluable discussions held with my colleagues; Allan Crowe, Gordon McClymont, Bill Milne-Home, Joao Kupper and Russel Finley. Many thanks for their comments and friendship.

A special thanks is due to Russel Finley for assisting me in performing many of the computer runs for this thesis. My sincere thanks is also extended to Elizabeth Szegvary of Acres International Limited who prepared most of the diagrams.

Funding for the project was provided by The University of Alberta in the form of teaching and research assistantships and by NSERC.

Finally, my deepest appreciation goes to my wife, Kathleen, for her continual support, encouragement, patience and constructive criticisms throughout this endeavour. To Kathleen and my children, Ryan and Lorna, my sincere apologies for the inordinate amount of time spent on this thesis; time which rightfully belonged to them.

TABLE OF CONTENTS

Chapter	Page
1. INTRODUCTION	1
2. INTERPRETING ELECTRICAL MEASUREMENTS	8
Formulation of the Interpretive Model	9
Conductance Considerations	17
3. SIMULATION OF DATA	21
Numerical Model	23
Boundary Conditions and Model Error	26
Electrode Configuration	32
Grid Design and Operation	33
Numerical Input	38
Analytical Output	46
Detection Criteria	46
4. SENSITIVITY ANALYSIS	48
Location of Anomaly	48
Size and Shape of Anomaly	66
Non-Uniform Medium	75
5. CONCLUSIONS	84
REFERENCES	87

LIST OF TABLES

Table	Description	Page
1	Summary of the Grid Design Parameters	37
2	Summary of the Anomaly and Medium Parameters. . .	41
3	Value or Description of the Parameters Used for the Reference Case (Trial A).	56
4	Trials Where the Position of the Anomaly is Varied.	58
5	Selected Crosshole Scan Results from Trial B. . .	62
6	Trials Where Anomalies With Different Sizes and Shapes are Varied	67
7	Selected Downhole Scan Results from Trials A, D, E and F.	71
8	Trials Where Additional Layers are Added to the Medium Representing Zones of Higher Resistivity	77

LIST OF FIGURES

Figure	Description	Page
1	Unit Section of the Electrode Grid Showing the Two Current Excitation Patterns. Note, in Application the "a" Spacing for the Crosshole Scans Will Usually Exceed that Used for the Downhole Scans	5
2	Relative Position of the Image Electrodes Used for Each Scanning Mode of Operation	16
3	Schematic Diagram Illustrating the Modeling Procedure	22
4	Boundary Effect on the Numerical Voltage (Wenner Array) for both the Downhole and Crosshole (Orthogonal) Scans. Analytical Voltage is Shown for Comparison	28
5	Selected Results from the Downhole Scans of a Uniform Medium Showing the Error in Apparent Resistivity over the Grid	30
6	Selected Results from the Crosshole Scans of a Uniform Medium Showing the Error in Apparent Resistivity Over the Grid	31
7	Model Grid Used for the Downhole Scans. The Dots Represent Electrodoes in Each Borehole	34
8	Model Grid Used for the Crosshole Scans. Note the Additional Cells which were Used to Expand the Bottom and Side Boundaries of this Grid Compared to the Grid Used for the Downhole Scans	36
9	Overall Structure of the Cell Assemblies Used to Represent Contaminant Plume Types 1, 2 and 3	39
10	Overall Structure of the Cell Assemblies Used to Represent Contaminant Plume Types 4, 5 and 6	40

Figure	Description	Page
11	Example of the Uniform and Gradational Internal Distributions of Conductivity Used for Anomaly S4. The Maximum Conductivity Ratio Between the Anomaly and Medium is 20 in Layer 3 for Both Distributions.	45
12	Variation in the aCR with the Position of Anomaly S3 Due to Downhole Scans across Layers 3 and 4	50
13	Variation in the aCR with the Position of Anomaly S3 Due to Crosshole Scans within Layer 3.	51
14	Selected Downhole and Crosshole Scan Results from Trial A	59
15	Selected Downhole and Crosshole Scan Results from Trial B	60
16	Selected Downhole and Crosshole Scan Results from Trial C	64
17	Selected Downhole Scan Results from Trials A, D, E and F.	68
18	Selected Crosshole Scan Results from Trials A, D, E and F.	69
19	Selected Downhole Scan Results from Trials C, G and H	73
20	Selected Crosshole Scan Results from Trials C, G and H	74
21	Selected Downhole Scan Results from Trials A, I and J Showing the Apparent Resistivity. . . .	79
22	Selected Downhole Scan Results from Trials A, I and J Showing the aCR Corrected with the Prevailing Background Conditions	80
23	Selected Downhole and Crosshole Scan Results from Trial K Showing the Effect of an Incorrect Use of the Background Conditions	82
24	Selected Downhole and Crosshole Scan Results from Trial K Corrected with the Prevailing Background Conditions. Compare These Results to Those Shown for Trial A'(Figure 14)	83

1. INTRODUCTION

One of the purposes of groundwater monitoring is to document, over time, any change in the groundwater chemistry. In the absence of a defined problem of contamination, monitoring wells are installed around all or part of the perimeter of a potential contaminant source. By carefully observing the long-term behavior of these wells in terms of particular contaminants, or certain "indicator" parameters, the development of a contamination problem will be apparent. In this manner, the wells serve as sentinel devices producing a reasonably effective warning system for the site. When a problem of contamination is known to already exist, monitoring with a system of properly located wells will document the pattern of continued spreading, or the success/failure of efforts to clean up the site.

Conventional monitoring in this manner is not without its limitations. First, the information from each sample is representative of only a small volume of the subsurface and therefore it is point-specific. Although point samples are desirable from the standpoint of accuracy and describing the position of a plume, they inherently have no capability of providing an early warning of the future arrival of a plume front. Unless a sufficient number of closely spaced wells are properly located near the potential contaminant source and are frequently sampled, the presence of a plume may go undetected until it reaches a considerable size. The resulting cleanup costs would therefore be higher than if the plume were detected sooner when it was less extensive. In fact, depending on how well the monitoring network

was laid out, a plume could go completely undetected. A second important limitation with conventional monitoring is the high ongoing operational costs. These costs include the manpower requirements for carrying out well purging and sample collection as well as the actual costs of performing the laboratory analyses.

Another possibility for monitoring is to employ some kind of electrical method. These techniques exploit the relation between increased electrical conductance and elevated dissolved solid concentrations usually associated with a contaminant plume. However, given the generally mixed record of success with surface techniques, it would be difficult to recommend that they be used for monitoring. The greatest problem is the ambiguities inherent in this method which arise mainly from its inability to:

(1) separate the influence on current flow produced by heterogeneities in the geologic medium from that produced by the variable distribution of the contaminant, without some form of geologic control (Klefstad et. al., 1975).

(2) resolve the electrical conductivity distribution in detail because by restricting the electrodes to the ground surface, neither current flow or voltage measurements can be focused about a plume at depth.

These two problems mean that a considerable amount of interpretative effort is required to produce even a relatively uncertain estimate of where a contaminant might be distributed. Delineation of a deep

plume is particularly difficult because the volume of the medium through which the current passes increases relative to the volume of the plume. This occurs because the separation of the electrodes must increase to provide appropriate penetration. Essentially, the plume exerts less and less of an influence on the electric potential with depth and therefore becomes masked in the process.

As a means of resolving the first problem, Hackbarth (1971) mapped the lateral variation in apparent conductivity prior to the introduction of a contaminant in the subsurface. By applying the concept of residual mapping he was able to examine the movement of a plume over time without the noise introduced by heterogeneities in the medium. He thus demonstrated the application of the electrical method as a true monitoring tool. One recent study which attempts to address the second problem regarding the resolution capabilities of the electrical method is the impedance computed system by Wexler and Mandel (1985). They described an inverse procedure which provides an estimate of the true conductivity distribution of a subsurface using an analogy with computed tomography as its theoretical basis. At this time, the main limitation in transferring its application from the laboratory to the field appears to lie in the assumption used in their algorithm of no-flow boundaries surrounding the perimeter of the subsurface grid (Tamburi et. al., 1985).

Borehole electrical methods appear to offer some important advantages over surface methods. However, they have been used only to a limited extent in contaminant studies because any borehole drilled could be better utilized as a monitoring device by completing it as a

well. Nevertheless, the main features of this approach are the ability to introduce current directly into the ground and, depending on the method, the opportunity to obtain precise vertical control on any variation in electrical conductance. This is in contrast to the surface method which is restricted to current excitation from the ground surface. Recently, Wilt and Tsang (1985) proposed an electrical method of mapping contaminant plumes using a borehole source and measurements of dipole voltages at the ground surface. Intended as an exploratory tool, they presented a series of simulations designed to show the sensitivity of the technique to various plume geometries and concluded improved results were obtained over surface arrays. This application is a continuation of the earlier work by Dey and Morrison (1979) in this field.

Given a means to resolve the deficiencies previously described for the surface method and noting that the borehole method is based on the same underlying theory as its surface counterpart, it should be possible for the electrical method to play a greater complementary role in monitoring. The goal of this research is to evaluate the feasibility of a new electrical technique for monitoring contaminant plumes in groundwater. The technique which is proposed here involves the use of a three-dimensional grid of electrodes installed permanently in the ground. Current can be introduced into the ground through any pair of appropriate electrodes comprising the subsurface grid (Figure 1) with the voltage recorded at the two intermediate electrodes. Using all possible combinations of neighboring electrodes, this operation could

Downhole Scan

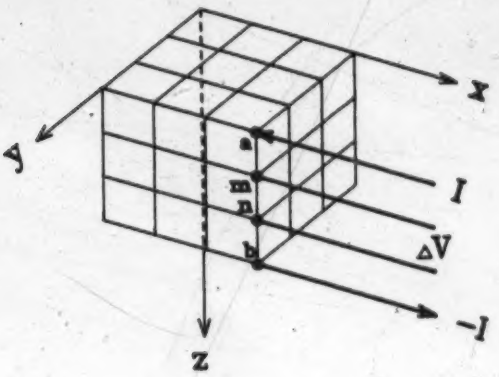

Crosshole Scan

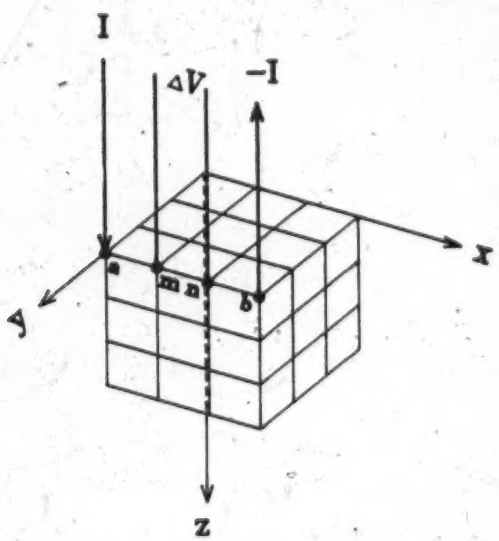

Figure 1. Unit section of the electrode grid showing the two current excitation patterns. Note, in application the "a" spacing for the crosshole scans will usually exceed that used for the downhole scans.

be repeated both in a downhole and crosshole manner, thereby scanning the entire region covered by the grid.

More specifically the objectives of this study are to:

(1) use a three-dimensional numerical model to simulate "hypothetical" electrical data under a known distribution of electrical conductivity.
(2) develop an analytical code to convert the set of electrical data into an apparent conductivity distribution.
(3) remove the influence of outside factors on the apparent conductivity distribution by employing the concept of residual mapping.
(4) undertake a sensitivity analysis to assess the performance of the technique.

This study is the first application of a new borehole electrical method. Its scope was therefore limited to theoretically evaluating the general concept of the technique without field or experimental validation. This approach was adopted in order that the test results could eventually serve as a guide for further work.

The advantages of this kind of system are readily apparent. By introducing a current into the ground using this proposed monitoring grid, electrical theory could be applied to resolve the apparent conductivity distribution in greater detail than offered by the surface method. Furthermore, if background conductivity conditions were obtained prior to contamination, the influence of the medium could be eliminated by mapping the residual conductivity (Hackbarth, 1971). This

technique is not viewed as a replacement for monitoring wells but rather is envisioned as an inexpensive and rapid means of handling most of the monitoring chores at a site. This would not only reduce the overall number of monitoring wells required, and hence the associated sampling costs, but would also provide between-point bulk conductivity information to accompany the point-specific chemical data given by wells. This latter argument emphasizes the technique as a leakage detection system. This permanent installation would be particularly appropriate for any type of liquid storage facility such as holding ponds or tanks where disruption of the monitoring grid is not anticipated following their installation.

2. INTERPRETING ELECTRICAL MEASUREMENTS

In this study, there are three important theoretical issues: (1) how an analytical expression can be used to interpret observed current and voltage measurements in terms of an electrical conductivity distribution; (2) how to deal with those variables which exert an influence on the determination of electrical conductivity and thus the successful delineation of a contaminant plume; and (3) how to simulate representative data resembling that which could come out of an actual field survey involving a contaminant plume. The first two questions are examined here while the third is discussed in the following chapter.

Electrical methods, which are based upon analytical solutions, have remained largely unchanged in concept since perfected by Schlumberger in 1912 (Kunetz, 1966). Only different electrode arrangements have been devised and the nature of the prospecting problems they have been applied to have varied over the years. Essentially, they can all be considered as an inverse technique, albeit simple ones.

As applied to an electrical method, an inverse problem is one of resolving the conductivity distribution of a medium, given a set of current and voltage measurements obtained from a particular electrode configuration. The following are the components of this inverse problem:

(1) the data set is the current strength and voltages measured at specified locations in, or on, a medium.

(2) the unknown parameter is the conductivity distribution of the medium.

(3) the model is the equation used to transform one into the other.

In this study, the evaluation of electrical measurements will be based on a conventional analytical method. The advantage in using this method over a more sophisticated inverse technique lies in its simplicity. It is a straightforward task to directly convert each set of current and voltage data into an apparent conductivity value. This calculation only requires the additional knowledge of where the current and potential electrodes are located relative to each other and the ground surface. By assembling a set of conductivity determinations made in three-dimensional space, the required overall distribution is obtained.

Other more sophisticated inverse methods do exist, such as the impedance computed system by Wexler and Mandel (1985). In this study, however, the analytical approach has been adopted because its usefulness has been demonstrated for years in a variety of studies. The numerical inverse techniques are much more difficult mathematically, and because of the sensitivity of the solution to features of the data set, can exhibit problems of instability.

Formulation of the Interpretive Model

Analytical expressions describing the distribution of the electric potential in a uniformly conducting medium due to the passage of a

steady direct, or low frequency alternating, current have been developed for both the surface and borehole electrical methods (see Jakosky, 1950 or Keller and Frischknecht, 1966). These expressions were derived from the point of view of being able to determine potential differences between points in a conducting medium, given its electrical conductivity and current strength. However, they can also be easily rearranged to yield the conductivity of the medium using measured voltages and known currents.

To begin a detailed discussion of the procedure used to develop the required analytical equation, consider now the equation of flow. The partial differential equation governing the three-dimensional steady state flow of current in an isotropic, homogeneous medium is the Laplace equation (Jakosky, 1950):

$$\frac{\partial^2 V}{\partial x^2} + \frac{\partial^2 V}{\partial y^2} + \frac{\partial^2 V}{\partial z^2} = 0 \qquad (1)$$

where V is the electric potential and x, y and z are the cartesian coordinates. Examination of this equation shows that the left side represents the sum of the rate of change in the electric potential gradients in the three principal coordinate directions while the right side indicates that charge is conserved. Together with the specified boundary conditions, a solution to equation (1) describes the distribution of the electric potential anywhere within a medium.

The starting point in obtaining an analytical solution to equation (1) is to examine only the flow of current due to either a point source

or sink in an infinite medium and consider this term as a boundary condition. Using a source and assuming that the outward flux of current is radially symmetric about the source, it is advantageous to express the Laplace equation in spherical coordinates with the source located at the origin. This form of the equation can be written as (Karplus, 1958):

$$\frac{1}{r^2}\frac{\partial}{\partial r}\left(r^2\frac{\partial V}{\partial r}\right) + \frac{1}{r^2\sin^2\beta}\frac{\partial^2 V}{\partial \alpha^2} + \frac{1}{r^2\sin\beta}\frac{\partial}{\partial \beta}\left(\sin\beta\frac{\partial V}{\partial \beta}\right) = 0 \qquad (2)$$

where r, β and α are the spherical coordinates. Because of the radial symmetry of the current flow, the derivatives, which account for the change in the voltage as a function of the coordinate angles, are zero. The resulting equation thus simplifies to:

$$\frac{1}{r^2}\frac{d}{dr}\left(r^2\frac{dV}{dr}\right) = 0 \qquad (3)$$

Total derivatives have replaced the partial derivatives since r is the only independent variable in the equation. Integrating this equation gives the following general solution:

$$r^2\frac{dV}{dr} = S \qquad (4)$$

and:

$$V = \frac{-S}{r} + C \tag{5}$$

The electric potential (V) is now simply a function of the radial distance (r) from the source, and the constants of integration (S and C) which must be evaluated in terms of the specified boundary conditions. The two boundary conditions are:

$$V = 0 \text{ at } r = \infty \tag{6}$$

$$\frac{dV}{dr} = \frac{-I}{A\sigma} \text{ at } r = 0 \tag{7}$$

where I is the current flowing through a cross-sectional area A in a medium of conductivity σ. The first boundary condition at the infinite boundary is a Dirichlet type boundary. If V approaches zero as r approaches infinity then, from equation (5), C must equal zero. Hence it can be eliminated from this equation. The second boundary condition at the source is a Neumann type boundary which is Ohm's law in differential form. Equating (7) with equation (4) gives:

$$\frac{dV}{dr} = \frac{-I}{A\sigma} = -\frac{S}{r^2} \tag{8}$$

therefore:

$$S = \frac{-Ir^2}{A\sigma} \tag{9}$$

For current flowing radially outward from a source, the cross-sectional area through which it flows is equal to the surface area of a sphere. This allows (9) to be rewritten as:

$$S = \frac{-Ir^2}{4\pi r^2\sigma} = \frac{-I}{4\pi\sigma} \tag{10}$$

Substitution of (10) into equation (5) then yields:

$$V = \frac{I}{4\pi r\sigma} \tag{11}$$

which is the desired specific solution to Laplace's equation. This solution relates the electric potential at any point in an infinite, uniform medium not only to the radial distance from the source, but also to the current strength at the source and the conductivity of the medium. Note from equation (11) that as r approaches zero, V approaches infinity and therefore the solution becomes invalid close to the source. It is for this reason that in applying equations of this form all electric potentials are analytically determined at points away from the source. In practice this also avoids problems of contact resistance at the current electrodes (Keller and Frischknecht, 1966).

Equation (11) also applies if current is withdrawn from a point sink. The only difference is a change in the sign of the equation. Hence this same equation can be used to derive the total potential at a point (m) due to both the source (a) and sink (b) by invoking the principle of superposition, or:

$$V_m = \frac{I}{4\pi\sigma}\left(\frac{1}{r_{am}} - \frac{1}{r_{bm}}\right) \tag{12}$$

where r_{am} is the distance from the source to point and r_{bm} is the distance from sink to point. To find the potential difference (ΔV) between two points, this approach is taken one step further by applying (12) to a second point (n) and then subtracting the results from each other. Hence, expanding this equation now gives:

$$\Delta V = V_m - V_n = \frac{1}{4\pi\sigma}\left[\left(\frac{1}{r_{am}} - \frac{1}{r_{bm}}\right) - \left(\frac{1}{r_{an}} - \frac{1}{r_{bn}}\right)\right] \tag{13}$$

or, rearranging it in terms of the conductivity:

$$\sigma = \frac{I}{4\pi\Delta V}\left[\left(\frac{1}{r_{am}} + \frac{1}{r_{bn}}\right) - \left(\frac{1}{r_{an}} + \frac{1}{r_{bm}}\right)\right] \tag{14}$$

Because equation (14) is developed for an infinite medium, it cannot be used where the source or sink are situated either on, or in close proximity to, a no-flow (Neumann type) boundary such as the ground surface. However, the effects of the boundary can be accounted

for using the method of images. Incorporating the image points shown on Figure 2, the equation is now:

$$\sigma = \frac{I}{4\pi\Delta V}\left\{\left[\left(\frac{1}{r_{am}} + \frac{1}{r_{bn}}\right) - \left(\frac{1}{r_{an}} + \frac{1}{r_{bm}}\right)\right] + \left[\left(\frac{1}{r_{a'm}} + \frac{1}{r_{b'n}}\right) - \left(\frac{1}{r_{a'n}} + \frac{1}{r_{b'm}}\right)\right]\right\} \quad (15)$$

Equation (15) is a general expression for the conductivity of a uniform medium which is semi-infinite in extent. It permits the current and potential points (electrodes) to be placed anywhere within the medium in any configuration. It is the same formula given by Daniels (1977) except that it is shown with derivation.

Figure 2 typically illustrates the location of the image electrodes relative to the ground surface for the two current excitation modes used in this study. The reference point for any conductivity calculation lies at the midpoint between the m and n potential electrodes. A conductivity anomaly is shown as the cross-hatched square in this diagram. Note that for the case where the electrodes are situated on the surface boundary, the additional image distance terms in equation (15) can be ignored and the 4π term in the equation reduces to the more familiar 2π term used in the surface method.

Although strictly valid only under the assumptions used to derive this expression, equations of this type are routinely applied to non-uniform regions of flow (i.e. containing varying types and forms of

Downhole Images

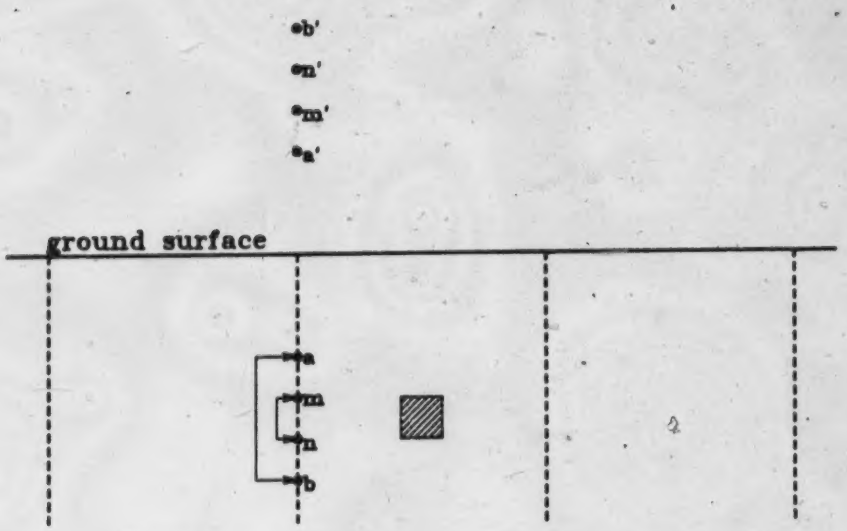

Crosshole Images

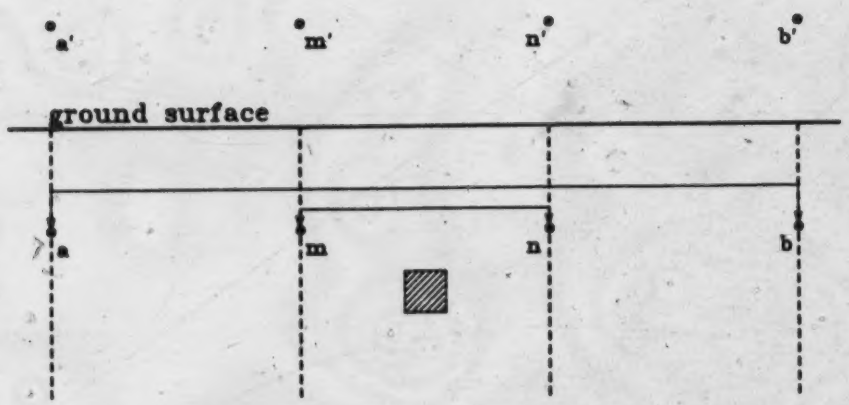

Figure 2. Relative Position of the Image Electrodes Used for Each Scanning Mode of Operation.

conductivity anomalies) with the qualification that the calculated conductivity represents an apparent conductivity.

Conductance Considerations

Before outlining the method used to generate the data set for this study, it is necessary to discuss the various factors which affect the determination of the bulk conductivity of a medium. These factors, some static and some variable, create the background conditions against which all subsequent monitoring data are compared. They must be recognized and properly handled, both in time and space, so as not to erroneously infer that any deviations in the data set are entirely due to the presence of a contaminant plume.

The conduction of an electrical current through an electrolytic porous medium is a function of several parameters, some of which are interrelated to one another. According to McNeill (1980), these include:

(1) mineral assemblage comprising the solid matrix, m (mainly the amount and type of clay minerals)

(2) size, shape and tortuosity of the void space, e (governed by arrangement and structure of solids)

(3) moisture content of the void space, ϕ

(4) amount and type of dissolved salts, c

(5) temperature of the pore fluid, T

Thus we have, $K = f(m,e,\phi,c,T)$

where K is the electrical conductance.

All of these parameters can in turn vary in space and the last three with time leading to a complex, three-dimensional, time-dependent distribution of K. The conductance decreases as the following decrease; the clay mineral content in m, the cross-sectional area in e normal to the flow of current, ϕ, c and T (particularly below the freezing point for water). Conduction increases as the length of the current path in e decreases.

When the electrical method is simply used to provide an estimate of the distribution of a contaminant at a particular time (i.e. a "snapshot" of a site), then the time variation in ϕ, c and T can usually be ignored. Also, if a representative background reading of the site is taken (for any given electrode spacing), then all measurements can be considered as deviations from this reading. This step effectively normalizes the data. Thus, the spatial variation in m, e, ϕ and T can also be neglected. Note, however, that this implies the geologic medium is homogenous. Nonhomogeneities, such as clay lenses, could locally influence the voltage readings and result in misleadingly high conductance values. Therefore, some form of confirmation of the physical characteristics of a site is usually required to verify the assumption of uniform conditions. If it is valid, then any remaining spatial variation in K can be attributed to c as a result of electrolytic displacement by a contaminating fluid.

In a monitoring application of the electrical method, those parameters that can vary over time cannot be ignored (i.e., ϕ, c and T). However, because the main interest in monitoring is to examine any variation in conductance at a particular point over time, each point will have its own unique set of background readings. Any spatial variation in the conductance parameters is therefore of no consequence because this will be individually reflected in the background data set. To successfully separate out the temporal influences on K, a suite of seasonal background readings will be required for each point prior to any contaminant being introduced into the subsurface. Thus, through judicious selection of the appropriate background reading at a given point, any change in K can again be attributed to c.

As an example of the aforementioned point, consider a site underlain by a sandy aquifer. It contains a shallow unsaturated zone with several clay lenses within the sands themselves. After installing the inground electrical grid, routine electrical measurements are collected over a period of time to establish the background conditions and any temporal variation in them. The static influence of the clay lenses always manifests itself in each set of electrical readings (and therefore is taken into account), while subsequent variations which are recorded largely reflect seasonal changes in the moisture and temperature conditions in the unsaturated zone. Following a leak from a storage tank on the site, an uncharacteristic voltage drop is observed in some of the readings. To highlight this, an appropriate set of background readings is selected and compared with the anomalous data. The residual conductivity approach clearly shows the presence of a

significant anomaly, an anomaly which is correctly attributed to a change in the dissolved solids content as opposed to other influences. If an incorrect set of background readings were used then the anomaly could have gone undetected through misinterpretation of the data or perhaps may have been dismissed as some unusual variation in the seasonal data.

3. SIMULATION OF DATA

An important aspect of this study is that the simulated data obtained from an electrical survey of various types of contaminant plumes reasonably represent field measurements. The approach adopted here has been to create this data set by using a three-dimensional numerical model. In effect, the model simulates the three-dimensional voltage pattern that would be produced by equipment in the field and the values an operator would record at the potential electrodes. Use of a numerical model enables any conductivity distribution to be constructed within the flow domain comprising the model grid. This flexibility makes it possible to examine systems involving different forms of contaminant plumes in a subsurface of varying geologic complexity. Hypothetical measurements using the electrode network were made in accordance with the scanning mode of operation described in Chapter 1.

Figure 3 is a flow chart which shows the overall modeling procedure. The hypothetical voltage measurements produced by the numerical model were used as input for the analytical solution. This was used to transform this data set into the resulting apparent conductivity distribution. The test of how well the permanently installed electrode system functions comes from evaluating a large number of model runs under a variety of conductivity distributions. It can then be determined to what extent the interpreted conductivity distribution matches the known original distribution.

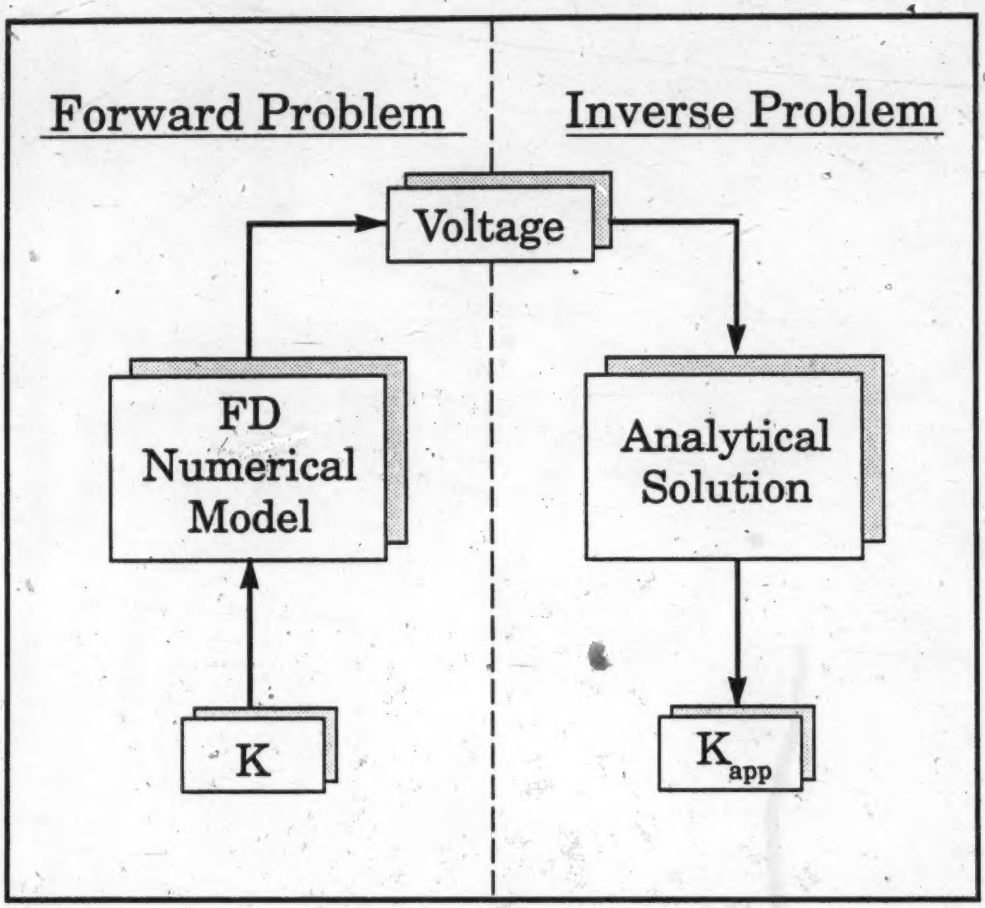

Figure 3. Schematic diagram illustrating the modeling procedure.

Numerical Model

A modified version of the groundwater computer code MODFLOW (McDonald and Harbaugh, 1985) was selected to simulate the three-dimensional voltage pattern. Although this code was developed to simulate groundwater flow it was easily adapted for this study on the basis of the analogy between the flow of groundwater and electrical current. As discussed by Rushton and Redshaw (1979), the following parameters are analogous: (1) electric potential and groundwater potential; (2) current and groundwater flow rate; and (3) electrical conductivity and hydraulic conductivity (electrical resistance is inversely proportional to transmissivity).

One advantage in using this code is that it is written in a convenient modular form. This feature permitted many of the options not required by this study to be easily removed from the program, thereby reducing the computer storage requirements. Another advantage is that the volumetric budget summary accompanying each numerical solution provides a check on the accuracy of the results.

Recall that the governing equation of flow used to develop the analytical solution was the Laplace equation. In applying this equation, the concept of apparent conductivity provides reasonable justification for disregarding heterogeneities in the medium thereby simplifying the assumptions concerning the properties of the region of flow. Furthermore, by partitioning the equation, sources and sinks were treated as boundary conditions rather than internally distributed energy within the medium.

In attempting to simulate realistic data with the numerical model, it is not sufficient to simply solve Laplace's equation for a homogeneous medium. This is because, for the sensitivity analysis, voltage is to be determined in a non-uniform medium containing internal sources and sinks. The governing equation of flow in this case is the Poisson equation:

$$\frac{\partial}{\partial x}\left(\sigma_x \frac{\partial V}{\partial x}\right) + \frac{\partial}{\partial y}\left(\sigma_y \frac{\partial V}{\partial y}\right) + \frac{\partial}{\partial z}\left(\sigma_z \frac{\partial V}{\partial z}\right) = i \qquad (16)$$

where σ_x, σ_y and σ_z are the electrical conductivity tensors in the three principal coordinate directions, i is the current per unit volume and the other terms have been previously defined. By subdividing the region into a three-dimensional grid, a finite difference approximation of Equation (16) can be written for each point in the grid.

By using known current and conductivity distributions and by specifying the boundary conditions, the resulting set of simultaneous equations can be solved for the electric potential using MODFLOW. Because the method is not restricted to simplifying assumptions, a wide variety of current patterns and electrical conductivity scenarios can be simulated.

Input to the code consisted of a specified distribution of electrical conductivity representing a natural system containing a conductive plume (an anomaly), and specified fluxes of current introduced at appropriate source and sink electrodes (nodes). Each simulation run actually involved a large number of measurements,

representing the compilation of data from all individual pairs of current and potential nodes. Thus, each run mimics an actual field survey where the location of the current electrodes is moved through the electrode network (numerical grid) while calculating the voltage drop between each of its intermediate potential electrodes. This systematic relocation of the current and potential nodal positions was done in both a downhole and crosshole manner. Thus, when in use during the scanning process, any given node within the grid can serve in a dual role; a current node during one voltage determination or a potential node during another. For each particular simulation, voltages were calculated for the entire region covered by the grid. However, only the voltage between the corresponding potential nodes was actually recorded as numerical output. The strongly implicit procedure (SIP) employing a block-centered nodal mesh was used as the solver for all simulations.

For reasons which will be subsequently discussed, two versions of the original MODFLOW code were made. One version was designed to carry out a complete sweep of the grid used for the downhole scans ("z" vertical direction). The other was devised for the grid used for the crosshole scans. The scanning directions for this latter version included the two orthogonal "x" and "y" directions and two 45 degree diagonal directions. The only significant modification required for each version of the code was the insertion of a number of DO Loops in the main program. These were placed in the code in order to repeatedly update the current and voltage nodal locations along the various

scanning directions during each run. This then automatically enabled a complete sweep of each grid to be made.

Boundary Conditions and Model Error

In the numerical model, a non-uniform conductivity distribution can be adequately represented by assigning particular values of conductivity in each cell surrounding the nodes of the grid. With respect to the boundary conditions, however, the model treats all outside boundaries of the grid as no-flow boundaries (unless otherwise specified). These boundary conditions pose a simulation problem because, in a real-world system, the boundaries are effectively infinite in all directions except for that above the ground surface. Care is therefore required to ensure that the model boundaries do not intrude on the solution. To address this concern, the approach which was followed was to expand the grid system horizontally and vertically away from that part of the domain in which the measurements were being made. Although this expanded system was not an infinite one, the boundary effects could be minimized.

The actual number of additional cells required to create a region of the appropriate size was determined using a set of simulated runs. For these runs, the source and sink nodes were fixed in one corner of a grid consisting of 25 columns, by 25 rows by 8 layers. This grid represents the size of the medium to be used for recording voltage measurements during the sensitivity analysis. For the downhole scans, the source and sink were located in layers 1 and 4 along column 1, row 1.

For the crosshole scans, they were positioned in columns 1 and 4 along row 1, layer 1. All runs involved the use of a conductivity of 0.01 mho/m for the medium, a current of 10 mA and a Wenner array employing "a" spacings of two and 12 m for the downhole and crosshole scans, respectively.

In each successive run, the size of the region was increased in a step-wise manner by adding an extra cell to each side and bottom boundary. In effect, shells one-cell in width were successively wrapped around the aforementioned grid thereby increasing the overall size of the flow domain. Eventually, no significant difference was observed in the voltage output between successive runs. From these serial test runs, it was found that seven additional shells per boundary would be sufficient to reduce the numerical-analytical error in the voltage to about 10 percent for the downhole scans. Numerical-analytical error is defined as the difference (expressed as a percentage) between the voltages predicted by each solution divided by the analytical, or true, voltage. Due to the greater "a" spacing of the crosshole scans, more shells were needed for this scanning mode. Eleven shells were required to reduce the error to about 13 percent for an orthogonal scan and about 30 percent for a diagonal scan. These additional shells represented the upper limit in terms of computer time and storage capabilities. Therefore, no further reduction in error due to the presence of the boundaries was possible for the crosshole scans using this array.

Figure 4 shows the effect of adding an extra shell to each boundary and the corresponding reduction in voltage for the downhole and orthogonal crosshole scans. All of the numerical results shown on

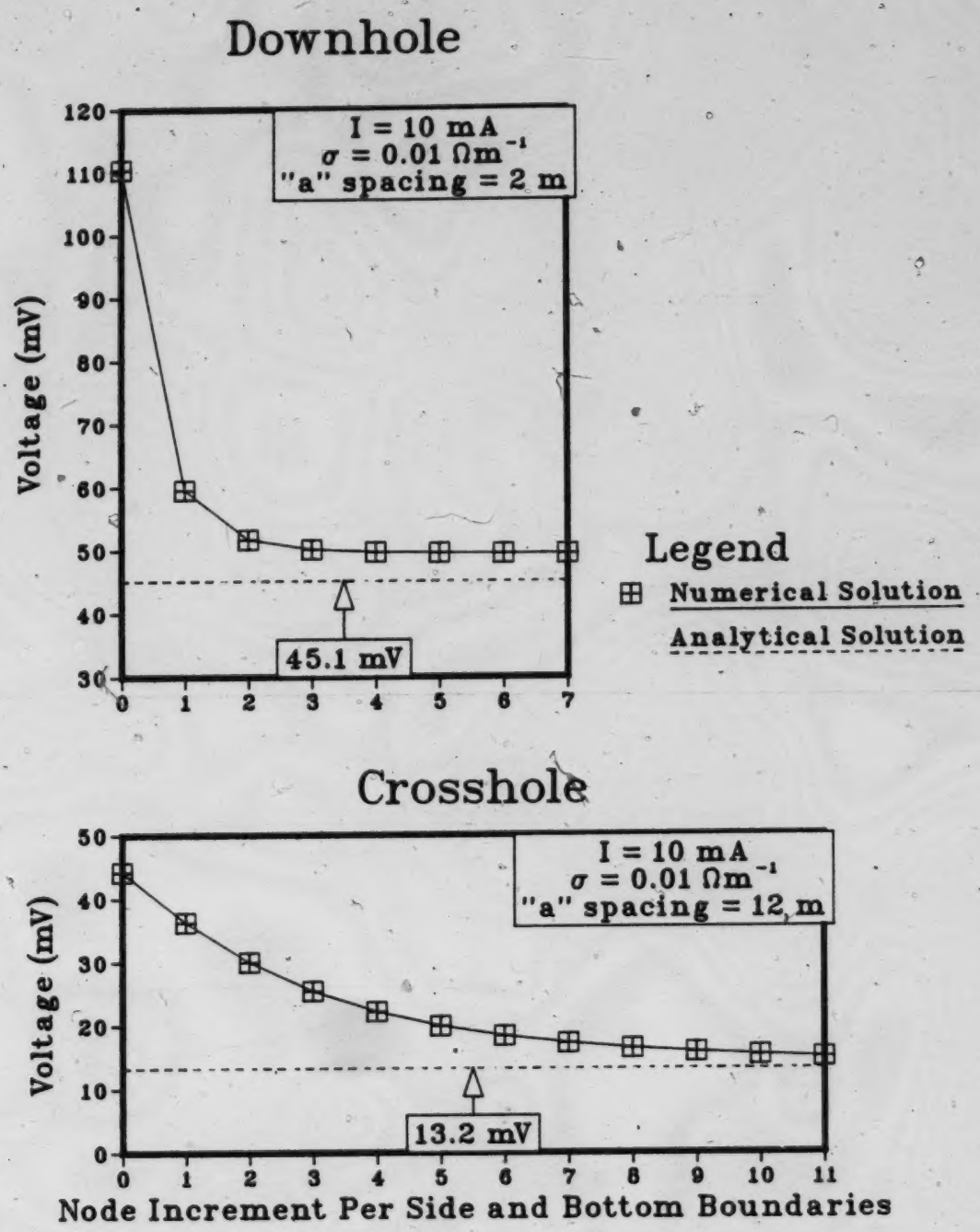

Figure 4. Boundary effect on the numerical voltage (Wenner array) for both the downhole and crosshole (orthogonal) scans. Analytical voltage is shown for comparison.

this diagram are the voltages recorded between the potential nodes intermediate to the source and sink nodes. The analytical voltage, which provides an exact solution to the problem, remains the same for all of the serial runs. As can be seen from this diagram, voltage decreases as the overall size of the flow domain increases. Because current is allowed to flow through a greater volume, the overall net resistance of the region is reduced and therefore the measured voltage is lowered. Nevertheless, some error will always remain. This is because the analytical solution applies to an infinite medium while the numerical results correspond to a finite medium which, through the addition of shells, only approximates an infinite medium.

The downhole scan results from Figure 4 are interesting in that an asymptotic value was reached after about four shells were added to each boundary. This suggests a part of the error arises from numerical discretization of the flow domain. For the most part, however, the error is considered to occur as a result of replacing an infinite medium with one that is finite in extent.

Figures 5 and 6 show that the error also varies with the position of the source and sink relative to the side and bottom boundaries of the grid. Both of these diagrams display the variation in apparent resistivity from two selected layers and one cross-section of the model grid. Resistivity, as opposed to conductivity, is shown strictly for presentation purposes. Figure 5 is for the downhole scans while Figure 6 is for the crosshole scans. The resistivity which was used as input was 100 ohm-m (conductivity of 0.01 mho/m). As can be seen, less error occurs as the source and sink approach the middle of the grid. There

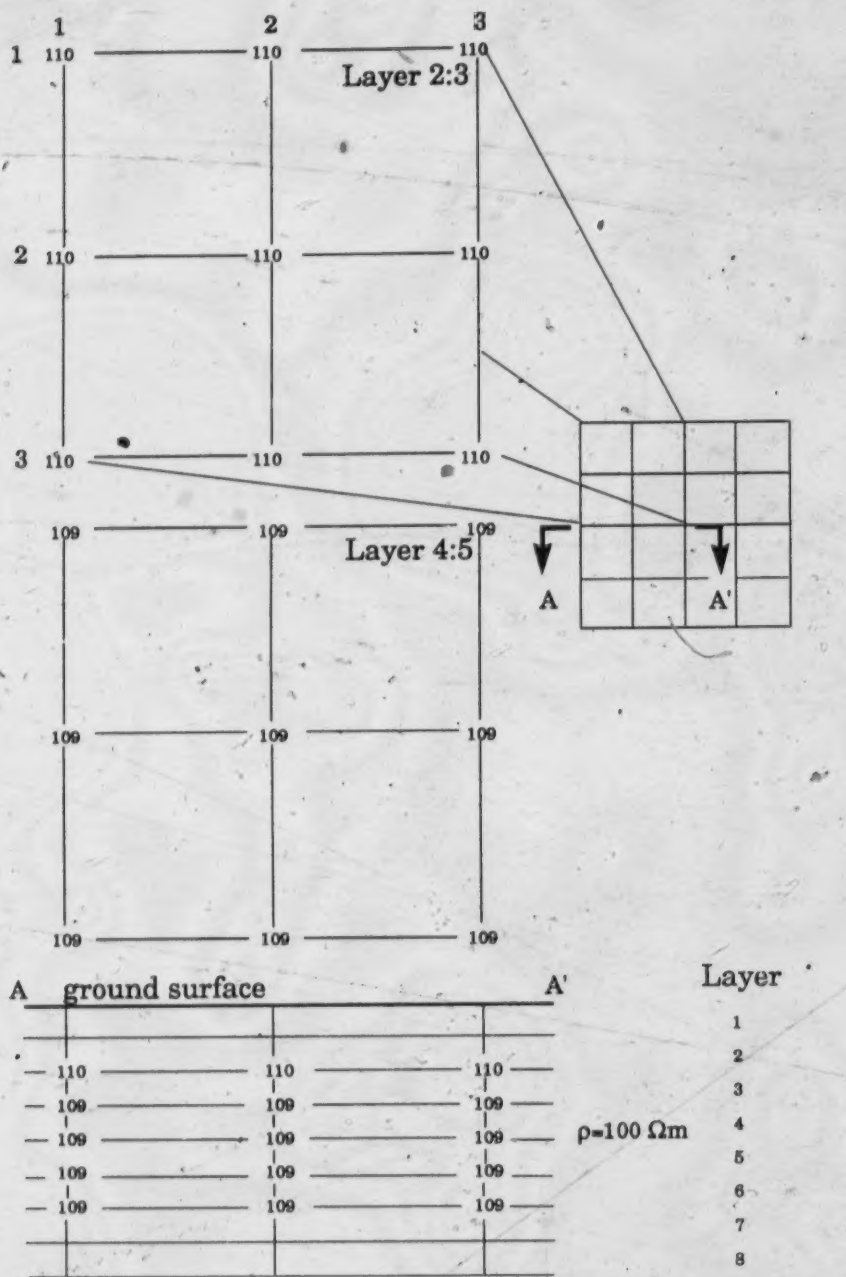

Figure 5. Selected results from the downhole scans of a uniform medium showing the error in apparent resistivity over the grid.

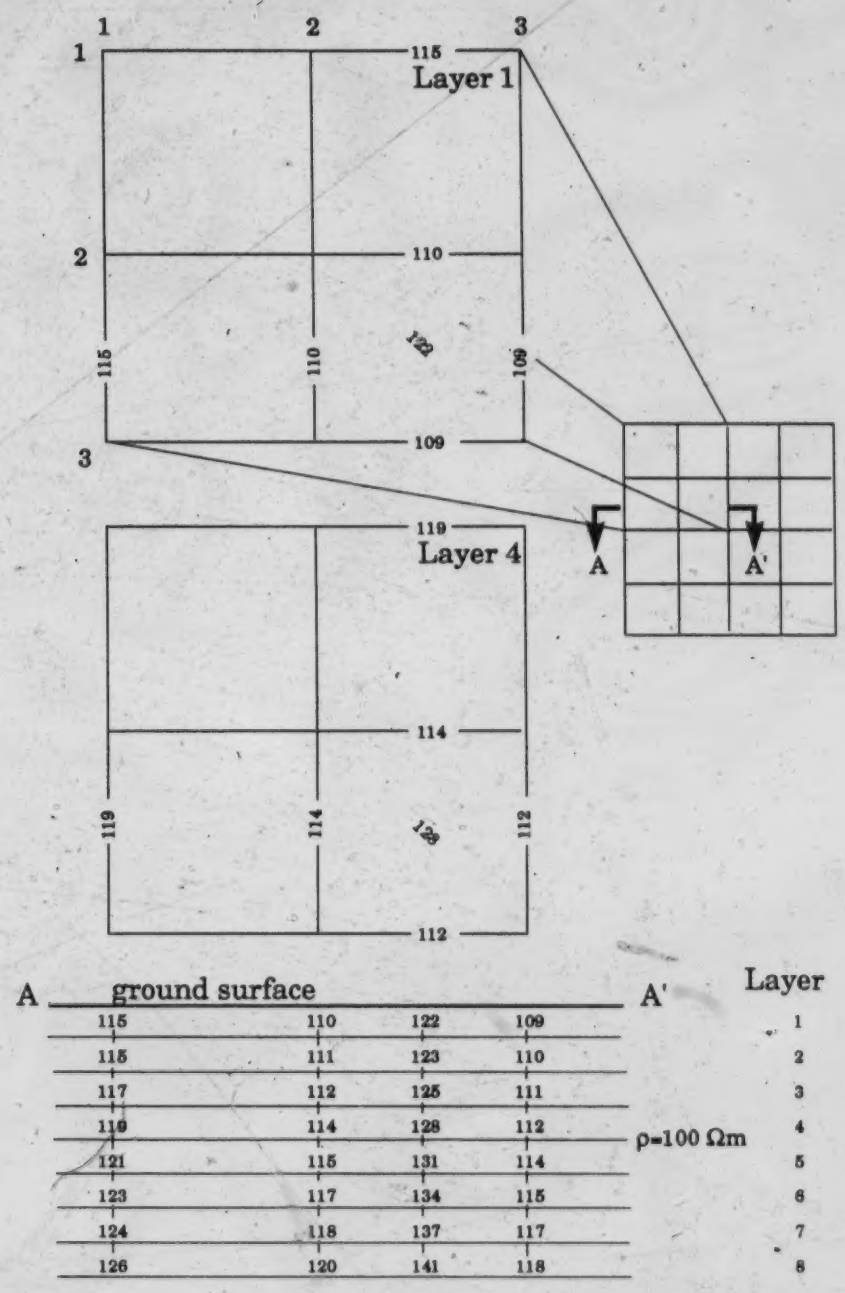

Figure 6. Selected results from the crosshole scans of a uniform medium showing the error in apparent resistivity over the grid.

is less tendency for the current to impinge on the outside boundaries. Note also how the resistivity increases as the current approaches the bottom boundary. This result is particularly evident for the crosshole scans.

Note that numerical-analytical error was assessed using a uniform medium. No attempt was made to analytically determine the error for a non-uniform medium. It is anticipated that an anomaly which is more conductive than the surrounding medium will result in less error than a medium that is entirely uniform. A more resistive anomaly, on the other hand, is expected to increase this error. It is for this reason that only more conductive anomalies were simulated in the sensitivity analysis. Nevertheless, for the purpose of this study the error in the results is considered to be consistent irrespective of whether the grid contains an anomaly or not (i.e. the error applies to all cases). The output should not be significantly affected provided the results are presented in a relative manner. This could be in the form of either a ratio or difference between the values obtained for an anomaly and the corresponding background readings.

Electrode Configuration

Two electrode configurations commonly used for the electrical method are the Wenner and Schlumberger arrays (Keller and Frischknecht, 1966). For a given node spacing in the model grid, the Wenner array requires a minimum number of four nodes for one solution, while the Schlumberger array needs at least six nodes. Up to this point all

electrical measurements were simulated using a Wenner array. Even by minimizing the source-sink nodal separation using this array, the numerical-analytical error could not be reduced below 10 percent. Therefore, without compromising the anticipated grid size to be used for the sensitivity analysis, it was impractical to use a Schlumberger array. This would have required an increase in the total number of nodes comprising the model grid for the same amount of voltage output.

Nevertheless, as a check on whether the use of a Schlumberger array would result in less error than the Wenner array, the step-wise boundary adjustment procedure was repeated for the former array using a downhole scan. The results indicated no significant difference occurred between the two arrays. Both overestimated voltage by about 10 percent.

Grid Design and Operation

On the basis of the preceding results, two model grids were designed for each scanning mode using a Wenner array; one for the downhole scans and the other for the crosshole scans. One grid could have been used for both scanning modes but this would have resulted in unnecessary computations, computer time and storage requirements. This is because the downhole scans need less additional shells per side and bottom boundaries than what is required for the crosshole scans.

The grid which was employed for all downhole scans consists of 39 columns, 39 rows and 15 layers (Figure 7). This node system can be subdivided into two parts. One part is the external or "boundary" part

Downhole Grid

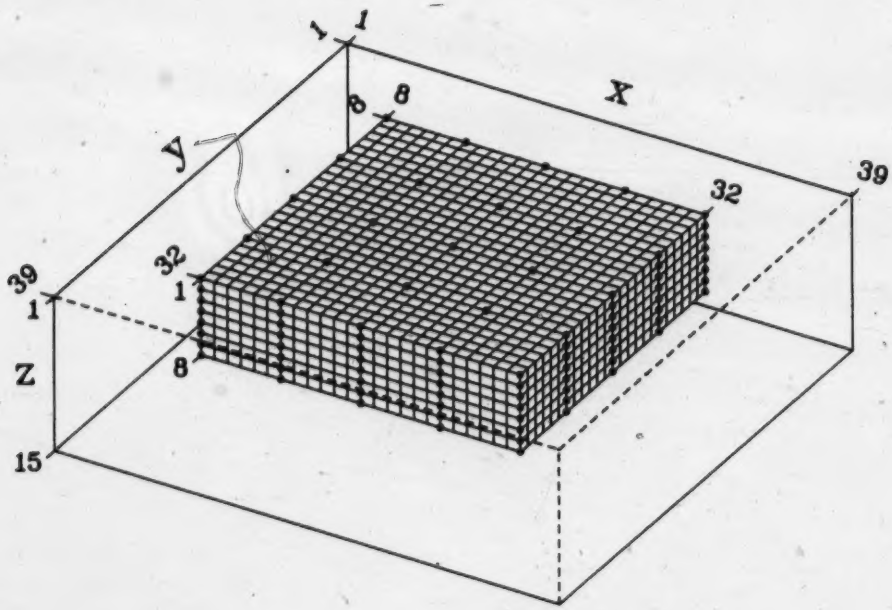

Figure 7. Model grid used for the downhole scans. The dots represent electrodes in each borehole.

of the grid which consists of the seven additional shells used to approximate infinite boundaries along the bottom and sides of the grid. The other part is an internal "test" grid used to evaluate this technique under the various conductivity scenarios. The test grid therefore consists of 25 columns, 25 rows and 8 layers.

The grid used for all crosshole scans consists of 47 columns, 47 rows and 19 layers (Figure 8). The boundary part of this grid contains eleven additional shells per side and bottom boundary. The test grid, however, remains the same for both scanning modes. Note that the node numbers for each test grid are different as a result of the change in their spacial origin.

Conceptually, each test grid can be further subdivided into a smaller "operational" grid containing 5 columns, 5 rows and 8 layers. This array of nodes represents the system of permanently installed electrodes placed in 25 boreholes (5X5) with 8 electrodes evenly distributed along each borehole. This operational grid is highlighted by the dots in Figures 7 and 8. If operated in the vertical, this arrangement results in five solutions per borehole (n-3) for a total of 125 downhole calculations. Operating in the horizontal results in 20 orthogonal and 8 diagonal solutions per layer for a total of 224 crosshole determinations.

Using cubic cells with dimensions of 2 m per side, the resulting test grid covers an area of 2,500 m^2 (50 X 50 m) and a depth of 16 m. The horizontal node separation between the boreholes is 12 m. Table 1 provides a summary of the grid design for each scanning mode of operation.

Crosshole Grid

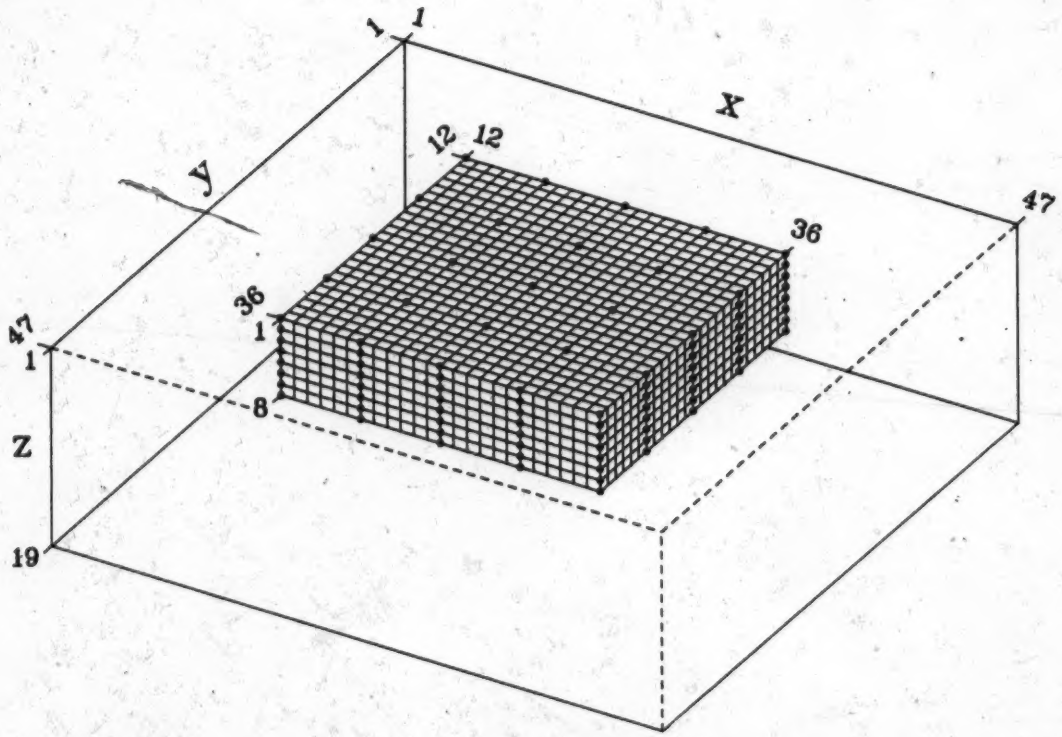

Figure 8. Model grid used for the crosshole scans. Note the additional cells which were used to expand the bottom and side boundaries of this grid compared to the grid used for the downhole scans.

TABLE 1. Summary of the Grid Design Parameters

Unique to Particular Scanning Mode	Downhole Scan	Crosshole Scan
overall grid (c,r,l)	39X39X15	47X47X19
number of additional shells per side and bottom boundary	7	11
Common to Both Scanning Modes		
resulting test grid (c,r,l)	25X25X8	
node spacing, m	2	
distance between scanning nodes		
-horizontal direction, m	12	
-vertical direction, m	2	
resulting operational grid (c,r,l)	5X5X8	

c,r,l - column, row, layer

Numerical Input

The different scenarios necessary to evaluate the efficacy of both the modeling concept and the interpretive technique can be created by selectively altering the conductivity distribution of the flow domain. This approach enables one to produce plumes with different sizes and shapes, adjust their position relative to the electrodes or vary their internal conductivity distribution. In a similar fashion, the remainder of the flow domain representing the medium can be left in a uniform state or can be modified to fabricate heterogeneities within the medium itself.

Plumes themselves were created by defining an arrangement of grid cells which, when collectively assembled, would represent a plume with a specified size and shape. Once placed in the grid, the conductivity of those cells comprising the plume were modified in accordance with the particular distribution to be used for a given simulation. Figures 9 and 10 illustrate, in three-dimensions, the cell assemblies devised for two small, spherical anomalies (S1 and S2) and four larger, ellipsoidal anomalies (S3 to S6). The term anomaly is used hereinafter in reference to a simulated groundwater plume. Table 2 summarizes the overall dimensions, resulting volumes and horizontal to vertical ratio between the major axes of each anomaly. All six were designed to represent plumes arising from a single episode, point source contaminant. The four larger, anomalies were created in an ellipsoidal manner in order to reflect the influence of a horizontally anisotropic medium on their shape. They were thus constructed such that their

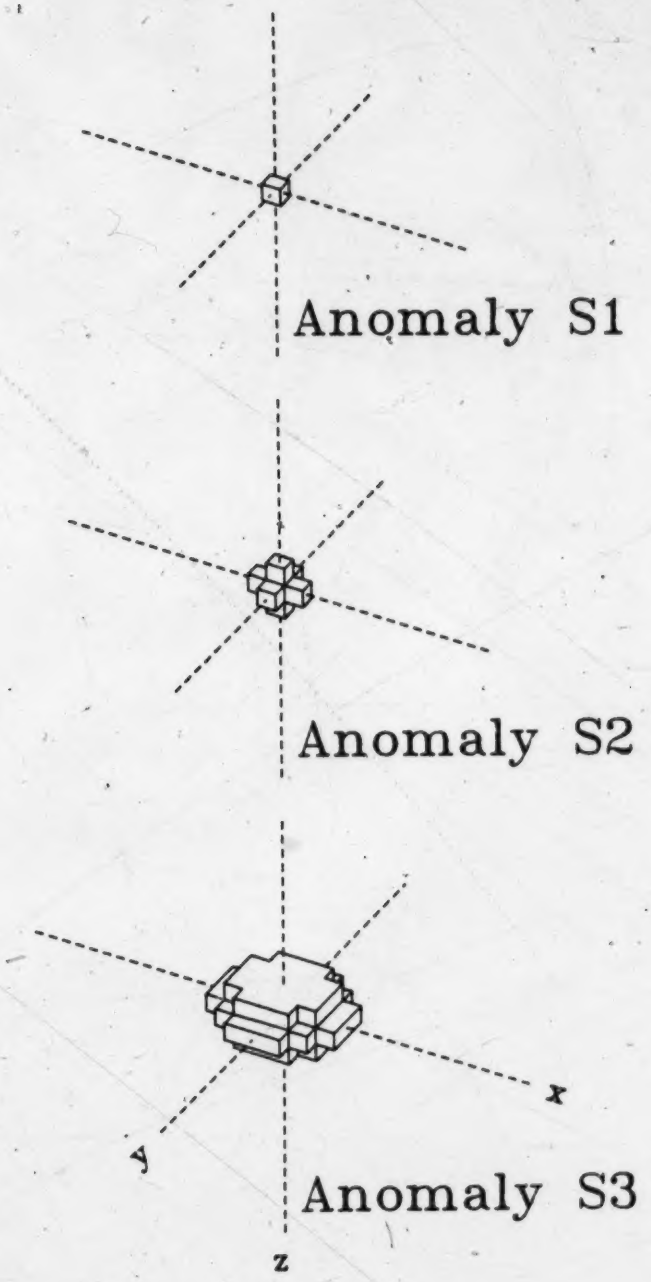

Figure 9. Overall structure of the cell assemblies used to represent contaminant plume types 1, 2 and 3.

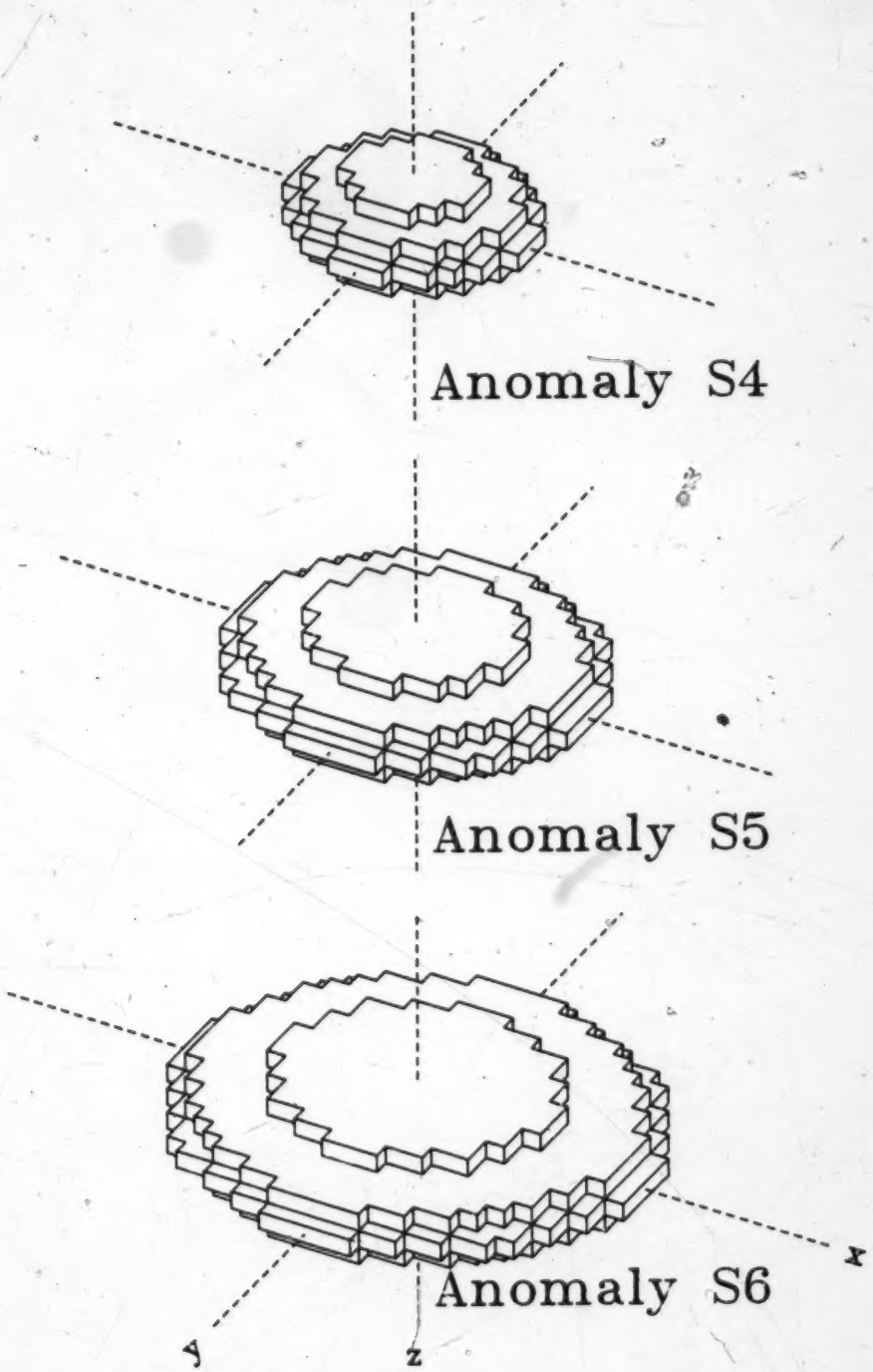

Figure 10. Overall structure of the cell assemblies used to represent contaminant plume types 4, 5 and 6.

TABLE 2. Summary of the Anomaly and Medium Parameters

Anomaly Parameters

Type	Shape	Overall Dimensions: Length m	Height m	Volume m^3	Horizontal to Vertical Ratio of Axes
S1	sphere	2	2	8	1:1
S2	"	6	6	56	1:1
S3	ellipsoid	14	6	79	3:1
S4	"	26	10	373	3:1
S5	"	38	10	897	4.5:1
S6	"	50	10	1,573	6:1

Type	Conductivity mho/m	Resistivity ohm-m
all anomalies (S1 to S6)	0.2	5

Medium Parameters

Material	Conductivity mho/m	Resistivity ohm-m
unsaturated - sand	0.002	500
- clay	0.005	200
saturated - sand*	0.01	100
- clay	0.2	5

*background value

extent in the horizontal direction (x and y) was greater than in the vertical (z). This was not practical for the two smaller anomalies. The circular symmetry of all of the anomalies with respect to their vertical axis was purposely maintained to reduce the computational effort required in any simulation run. By taking advantage of the symmetry of an anomaly less measurements would have to be made during the scanning process. This simplified the simulations and avoided duplication in the numerical output.

The position of an anomaly within the grid was determined by simply placing the origin of its three major coordinate axes (x,y and z) at a location of interest. The limits of each anomaly with respect to the test grid were then established and the conductivity of each cell was adjusted as previously described. These positions could represent the occurrence of a plume arising from either the introduction of a contaminant into the subsurface at different locations or, in comparison to each other, the effect of its migration over time. For the reasons previously outlined, anomalies were located in positions which were symmetrical with respect to the operational grid. This then avoided duplication in the numerical output during the scanning process.

For convenience, the method used to describe the position of an anomaly with respect to the operational grid was to note the position of either its vertical axis and/or horizontal central plane. For example, an anomaly positioned in the middle of the 5X5X8 operational grid between layers 4 and 5 would be described as being situated at position 3,3,4:5. The first two numbers refer to the column and row

coordinates of its vertical axis while the third number indicates the layer coordinate of its horizontal central plane. A colon is used to specify a location half way between any two coordinates; in this case between the two layers.

Two different styles of internal conductivity distributions were used for the anomalies; a uniform and a gradational one. For the uniform distribution, a conductivity 20 times that of the medium was used for all cells representing an anomaly. This value corresponds to a conductivity of 0.2 mho/m, or 5 ohm-m of resistivity. Although it is difficult to place a corresponding total dissolved solids concentration on this figure, a review of the literature (Reed et. al., 1981; Cartwright and McComas, 1968) suggests between 1000 and 10,000 mg/L may be appropriate. The uncertainty in this range stems from differences in the geologic conditions (see discussion under "Conductance Considerations") and "a" spacings used in the aforementioned studies with that theoretically adopted for this project. Thus, the maximum conductivity of the anomalies is representative of values observed in many different types of contamination problems. For a gradational distribution, only the central cell of an anomaly (origin of its three coordinate axes) had a conductivity contrast of 20 with the medium. The conductivity of the remaining cells declined uniformly to the perimeter of the anomaly in accordance with the following equation:

$$\sigma = \sigma_{max} \exp\left(-\frac{a^2}{m_1} - \frac{b^2}{m_1} - \frac{c^2}{m_2}\right) \qquad (17)$$

where a,b and c are the distances from the centroid of the anomaly to a particular cell in the three principal coordinate directions and m_1 and m_2 are empirical constants. These constants were determined on a trial and error basis until the conductivity of the cells bordering the perimeter of an anomaly matched the background value of 0.01 mho/m used for the medium. The m_1 denominator in the exponent was used for both the x and y directions because conductivity was varied equally in these two directions.

Figure 11 is a three-dimensional diagram showing the difference in these two distributions using anomaly S4 as an example. The three layers shown represent the top three layers of this anomaly which, in this example, is horizontally positioned in the middle of the test grid. For the complete distribution, layers 1 and 2 would be repeated below the central plane as layers 5 and 4, respectively. The gradational distribution was used for most of the simulations in the sensitivity analysis because it was considered to be the more realistic one. This distribution was designed to represent the effects of dispersion on the concentration of a contaminant within the anomaly. The uniform distribution was only used in some of the preliminary simulations or, for size reasons, on the two smaller anomalies.

Non-uniform media were simulated by replacing all, or in part, one or more layers of the medium with a different conductivity. For example, an unsaturated zone could be represented by lowering the conductivity of the top several layers. Similarly, the effect of a lens of different material in the medium could be created by changing the conductivity of part of a layer. Representative conductivity values

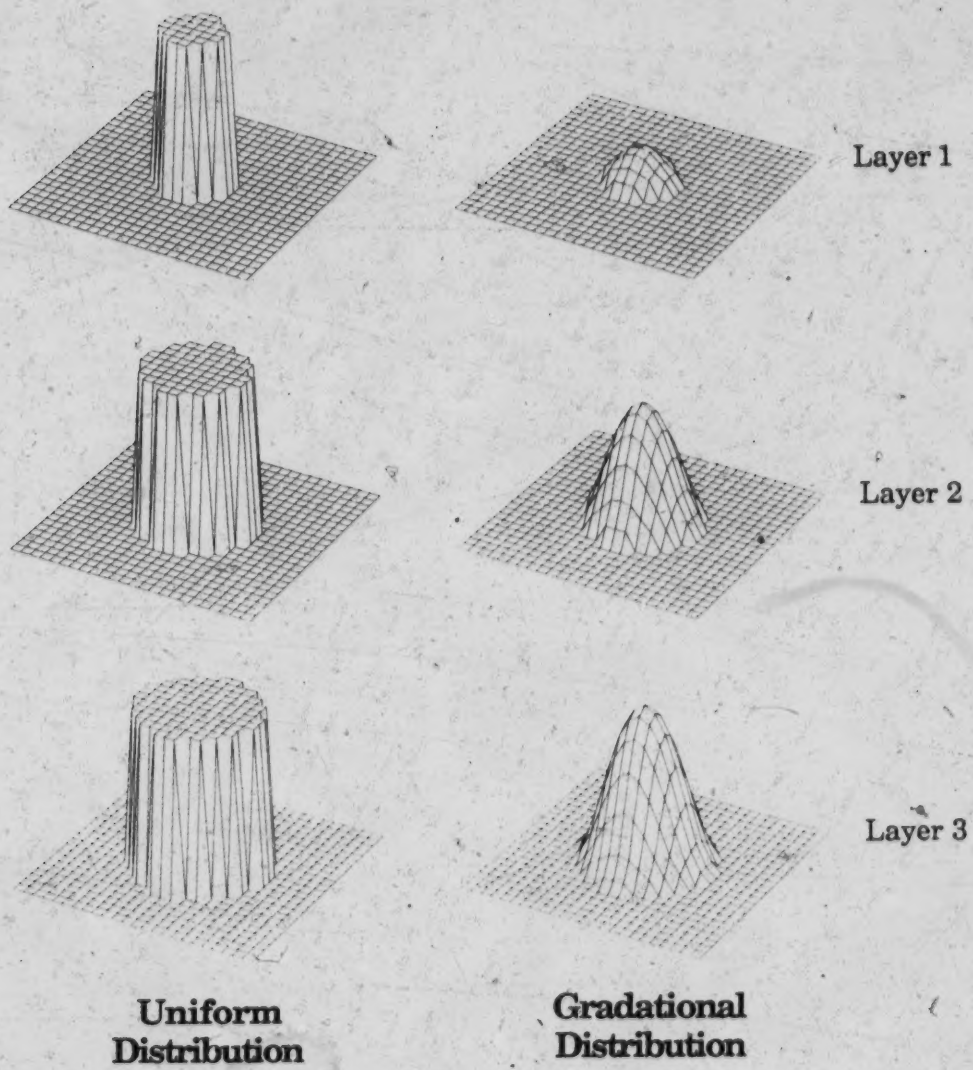

Figure 11. Example of the uniform and gradational internal distributions of conductivity used for anomaly S4. The maximum conductivity ratio between the anomaly and medium is 20 in Layer 3 for both distributions.

used for fabricating non-uniform media are summarized at the bottom of Table 2. These are typical values which could be encountered in the field (Jakosky, 1950).

Analytical Output

The voltage data created by the numerical model is assumed to provide the equivalent of a set of monitoring data that one might collect from a field site. Interpreting these data involves the application of the analytical approach described in Chapter 2.

A computer code was written to convert all voltage output provided by the numerical model into the corresponding apparent conductivity. Analytical output was provided in two forms:

(1) the predicted apparent conductivity (aC), in mho/m

(2) the residual apparent conductivity expressed as a ratio (aCR) between the predicted and background apparent conductivities, dimensionless

Detection Criteria

In using the residual conductivity approach, it was necessary to define what difference in conductivity should be considered as significant. In other words, if real data were measured in the field then some variation in the background readings would be expected as noise. If this were taken into account then what amount of residual

conductivity must be present before one could say with some confidence that the results represent the presence of a plume. A review of the literature (Klefstad et. al., 1975; Reed et. al., 1981) suggests that if anomaly and medium resistivities of 5 and 100 ohm-m, respectively, were used in the simulations then a residual difference of 10 ohm-m could be considered as significant. When expressed as a ratio, this corresponds to a value of 1.1. Therefore for the purpose of the sensitivity analysis any values below this were considered as questionable in terms of their significance. This ratio could also be thought of as the detection criteria for the study.

4. SENSITIVITY ANALYSIS

In the sections that follow, the application of the proposed monitoring technique is evaluated in terms of its ability to detect and delineate anomalies. All of the tests involve how well the hypothetical inground electrode network is able to detect the presence of a plume. The simulated measurements are interpreted using the analytical expression (15). The predicted apparent conductivity pattern resulting from this expression is compared with the actual conductivity distribution used as numerical input.

The trials comprising the sensitivity analysis consist of examining the effects of: (1) varying the location of an anomaly relative to the grid network; (2) placing anomalies with different sizes and shapes within the grid; and (3) using a more complex medium containing different types of heterogeneities. One effect not examined independently was varying the internal distribution of conductivity. Most trials contained anomalies with a gradational distribution, as opposed to a uniform one, because this was felt to be the more realistic distribution to model.

Location of Anomaly

A series of preliminary trials are presented in order to establish whether the interpreted conductivity pattern depends on the horizontal position of an anomaly. These trials involved the use of the same size test grid as for the complete sensitivity analysis (see Figures 7 and

8), except that it was partitioned into a 4X4X5 operational grid instead of a 5X5X5. This change enabled more detailed horizontal positioning of an anomaly with respect to the operational electrodes (i.e. boreholes) because 8, as opposed to 6, cells were now situated between these electrodes. Note, however, that the size of the overall grid for each scanning mode remained the same.

The results of five trials with anomaly S3 are illustrated in Figures 12 and 13. In these trials, the vertical axis of this anomaly was repositioned in a systematic way. The axis was moved from electrode 3,3 in example (c), to two intermediate locations between neighboring electrode 2,2 along the diagonal [examples (a) and (b)] and, similarly, two intermediate locations between electrode 2,3 in an orthogonal direction [examples (d) and (e)]. Figure 12 is the predicted aCR in plan view for the downhole scans across layers 3 and 4 while Figure 13 is the same view for the predicted aCR arising from the diagonal and orthogonal crosshole scans within layer 3. For all cases the conductivity distribution within the anomaly was a uniform 20:1 conductivity ratio (CR) with the medium (100 ohm-m resistivity) while the horizontal central plane of the anomaly was always positioned within layer 3.

Beginning with the downhole scans, Figure 12(a) is an example of a situation where the anomaly, although significant both in size and conductivity contrast with the medium, remained undetected by the four surrounding electrodes even though they are situated close to its edge. Compare this result with the examples shown in Figure 12(b), (c) and (e) in which a portion of the anomaly passes through electrode 3,3. In

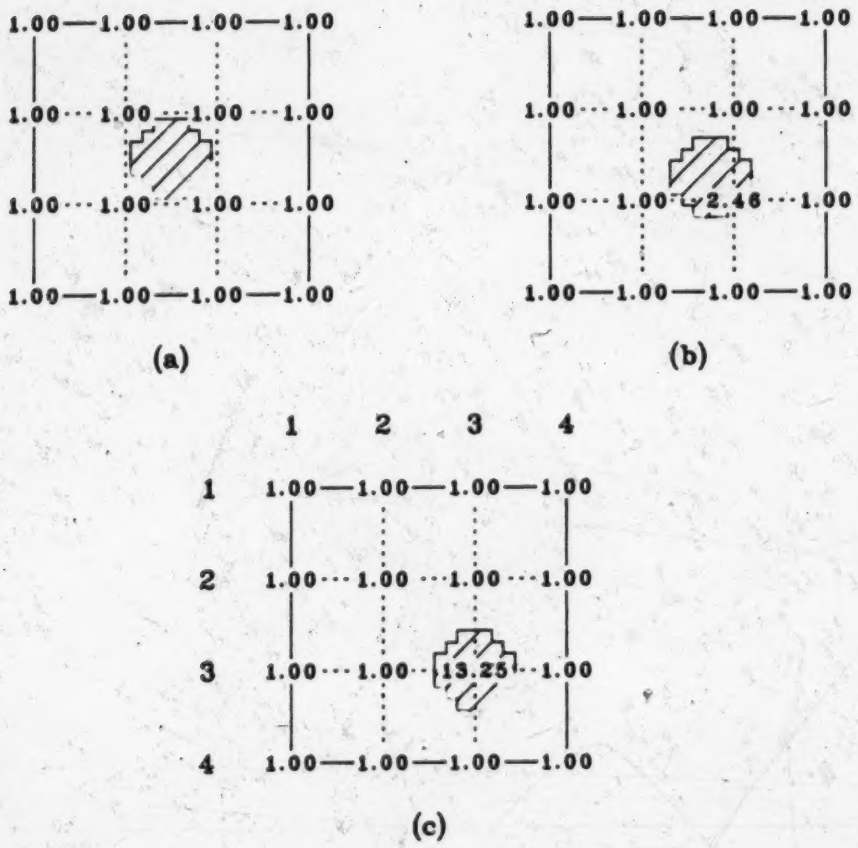

Figure 12. Variation in the aCR with the position of Anomaly S3 due to downhole scans across Layers 3 and 4.

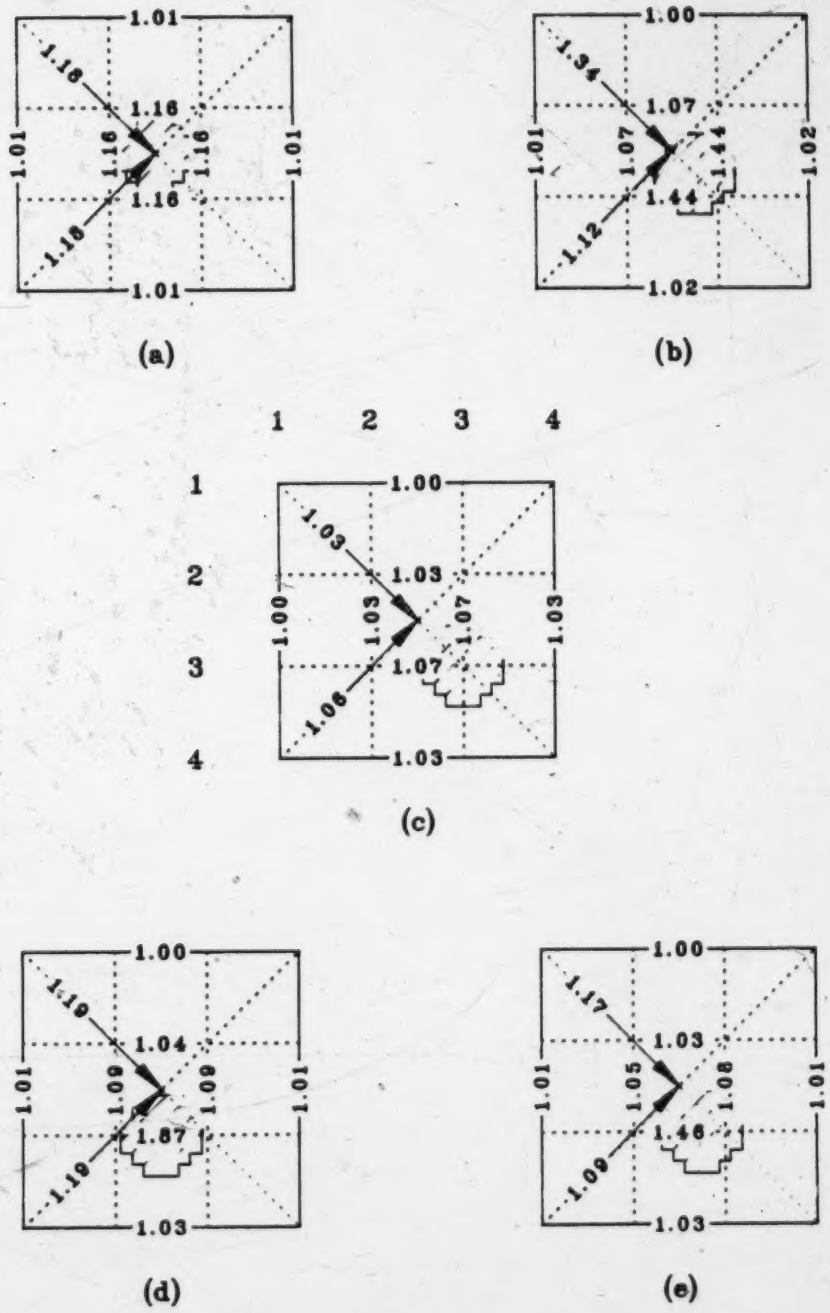

Figure 13. Variation in the aCR with the position of Anomaly S3 due to crosshole scans within Layer 3.

each of these examples the anomaly has been detected because one of the downhole scans passes through a portion of the anomaly. This result indicates that at an "a" spacing of 2 m the downhole scans may not always detect an anomaly but it does serve to delimit the probable horizontal extent of one. Note also how the predicted aCR improves in value as the vertical axis of the anomaly approaches electrode 3,3.

The difficulty, however, which still remains with these latter three examples is that neither the size nor exact horizontal position of the anomaly can be inferred with only one electrode. Based solely on this information, any number of anomalies of undetermined size could be similarly situated anywhere within the area immediately surrounding electrode 3,3. Turning now to Figure 12(d), this example is a case in which the anomaly has been marginally detected by two electrodes adjoining it. The anomaly can now be inferred to lie equidistant between these two electrodes but again its size and exact position remained undetermined.

The results from these trials clearly show that vertical scanning is insufficient by itself. Additional information is required to determine the horizontal position of the anomaly or, in some cases, determine if it is to be detected at all. This additional information could be provided in several different ways. More electrodes comprising the operational grid could be installed, thereby improving its resolution capabilities, or perhaps a reduced number of downhole scans could be repeated at a larger "a" spacing. Before resorting to this, however, the same set of examples were reexamined in terms of the information obtained through crosshole scans.

Figure 13 illustrates the predicted aCR as given by orthogonal and diagonal crosshole scans of the anomaly in the five positions discussed previously. In example (a), the anomaly is now detected, albeit marginally, and can be inferred to be centrally located between the four surrounding electrodes. This is based on both this scan pattern and the downhole scan results. Recall that the results from the downhole scans could not in themselves detect the anomaly, but the information could be used to limit its horizontal extent.

For example (c), in which the central axis of the anomaly is situated about electrode 3,3, the predicted aCR results from the orthogonal and diagonal crosshole scans [Figure 13(c)] indicate that the anomaly is positioned about this electrode. Strictly speaking, these results do not in themselves entirely demonstrate the exact horizontal position of the anomaly but, given a more complete set of output data utilizing a larger operational grid, this can easily be inferred from the diagram. However, the magnitudes of the predicted aCR values shown on Figure 13(c) are such that the degree of confidence in the results is questionable. All values fall below the detection criteria of 1.1. Recall that this criteria corresponds to a residual resistivity of 10 ohm-m. A value less than this was considered to be within the noise that might ordinarily accompany background readings. Hence, it cannot be said with any certainty whether a ratio this small represents background scatter or the possible presence of a plume. This example serves to demonstrate that crosshole scans may not necessarily be able to resolve the exact horizontal position of an anomaly despite the fact that the downhole scans [Figure 12(c)] clearly indicated its presence.

In the remaining trials where the vertical axis of the anomaly is not fully symmetric with respect to the grid [Figures 13(b), (d) and (e)], some of the results from the crosshole scans are sufficient to indicate its relative horizontal position. In example (b), the corresponding predicted aCR values in the two orthogonal directions indicate the anomaly is horizontally symmetric about the diagonal axis between electrodes 2,2 and 3,3 and that its vertical axis is closer to the latter electrode. However, it is recognized that most of the predicted aCR values from the orthogonal scan for this example are below the detection criteria. As mentioned for example (c), a larger operational grid would not only provide the additional orthogonal and diagonal scan results to support this inference of the position of the anomaly but would also enable a clear distinction to be made between examples (b) and (c). Continuing with examples (d) and (e), note how one set from each of the orthogonal scans indicates the vertical axis of the anomaly lies along the axis joining electrodes 2,3 and 3,3 while the other orthogonal set and the predicted aCR from the diagonal scan can be used to infer its position between these two electrodes. However, as with the previous examples, examples (d) and (e) would also require more information from a larger operational grid in order to fully deduce the position of the anomaly.

The results from this set of preliminary trials demonstrate that the predicted aCR results from the downhole and crosshole scans can be used in combination with each other to infer the horizontal location of an anomaly. This is provided a suitably sized anomaly with a sufficient conductivity contrast with the medium is present. Improved aCR values

generally occur as a greater portion of the anomaly lies between any two potential nodes, whether operating in a downhole or crosshole manner. It is the differences or similarities in the magnitude of these results which enable the horizontal position of the anomaly to be inferred. The crosshole scans provide more information about the horizontal position than downhole scans but are limited in that the magnitude of the aCR values is small due to the greater "a" spacing used. Downhole scans themselves are not conclusive in resolving the position of an anomaly in the horizontal but can be used to limit its probable extent as suggested by a crosshole scan pattern. Depending on the position of an anomaly, downhole scans can also provide better estimates of the actual CR due to a smaller "a" spacing and therefore more focused current excitation.

The next part of this section is concerned with the apparent conductivity pattern which occurs as a result of varying both the horizontal and vertical position of an anomaly. These cases differ from the preliminary trials in that all results are now compared with a reference case. Two points were considered in developing this. First, the preliminary trials revealed that a larger anomaly would be required if the capabilities of a vertical scan were to be fully explored. Therefore, Anomaly S4 was selected. Second, for an anomaly of this size it would also be more realistic to use a gradational distribution of conductivity within the anomaly itself.

Table 3 is a summary of the parameter values and descriptions used for the reference trial (Trial A). The characteristics of the medium used for the preliminary trials were retained for the reference

TABLE 3. Value or Description of the Parameters Used for the Reference Case (Trial A)

Parameters	Value or Description
Anomaly Parameters	
type	S4
overall dimensions - length (x,y), m	26
- height (z), m	10
volume, m^3	373
shape	ellipsoid
ratio of horizontal to vertical axis	3:1
resistivity, ohm-m	5
internal resistivity distribution	gradational
location of centroid with respect to operational axis - x_o, y_o	column 3, row 3
- z_o	layer 4
Medium Parameters	
resistivity, ohm-m	100
resistivity distribution	uniform
Excitation Parameters	
current, mA	5
array type	Wenner

simulation while, as a result of using a gradational distribution, the 20:1 CR becomes the maximum value between the centroid of the anomaly and the medium. All subsequent analyses were also performed with the complete 5X5X8 operational grid in order to provide additional excitation points and thus more detailed crosshole data which was lacking in the previous trials. Note that the horizontal central plane of the anomaly was also moved down from layer 3 to layer 4.

Three simulations (Trials A to C) were carried out to examine the effect of horizontal and vertical positioning of anomaly S4 on the predicted aCR. A summary of the changes in the positioning of the anomaly for these trials is presented in Table 4. The two horizontal positions used were the same for examples (a) and (c) in the preliminary trials (i.e. the vertical axis of the anomaly was situated at horizontal positions 3,3 and 2:3,2:3, respectively). For the vertical positioning, the horizontal central plane was situated either in the middle of layer 4 or between layers 4 and 5.

Figures 14 and 15 respectively display the predicted aCR results obtained from the downhole and crosshole scans of Trial A (reference simulation) and Trial B. In this latter simulation, the horizontal central plane of the anomaly is moved down half a layer compared to the reference case. The top diagrams are a plan view of the crosshole scan results through layer 4 while the bottom diagrams illustrate, in cross section, the downhole scan results along one of the orthogonal planes passing through the anomaly's vertical axis.

The interesting feature to note from a comparison of the two downhole scan results is the vertical symmetry displayed by the

TABLE 4. Trials Where the Position of the Anomaly is Varied

Parameter	Trial A	Trial B	Trial C
location of centroid of anomaly S4 with respect to operational grid			
- x_o, y_o	3,3	3,3	2:3,2:3
- z_o	4	4:5	4

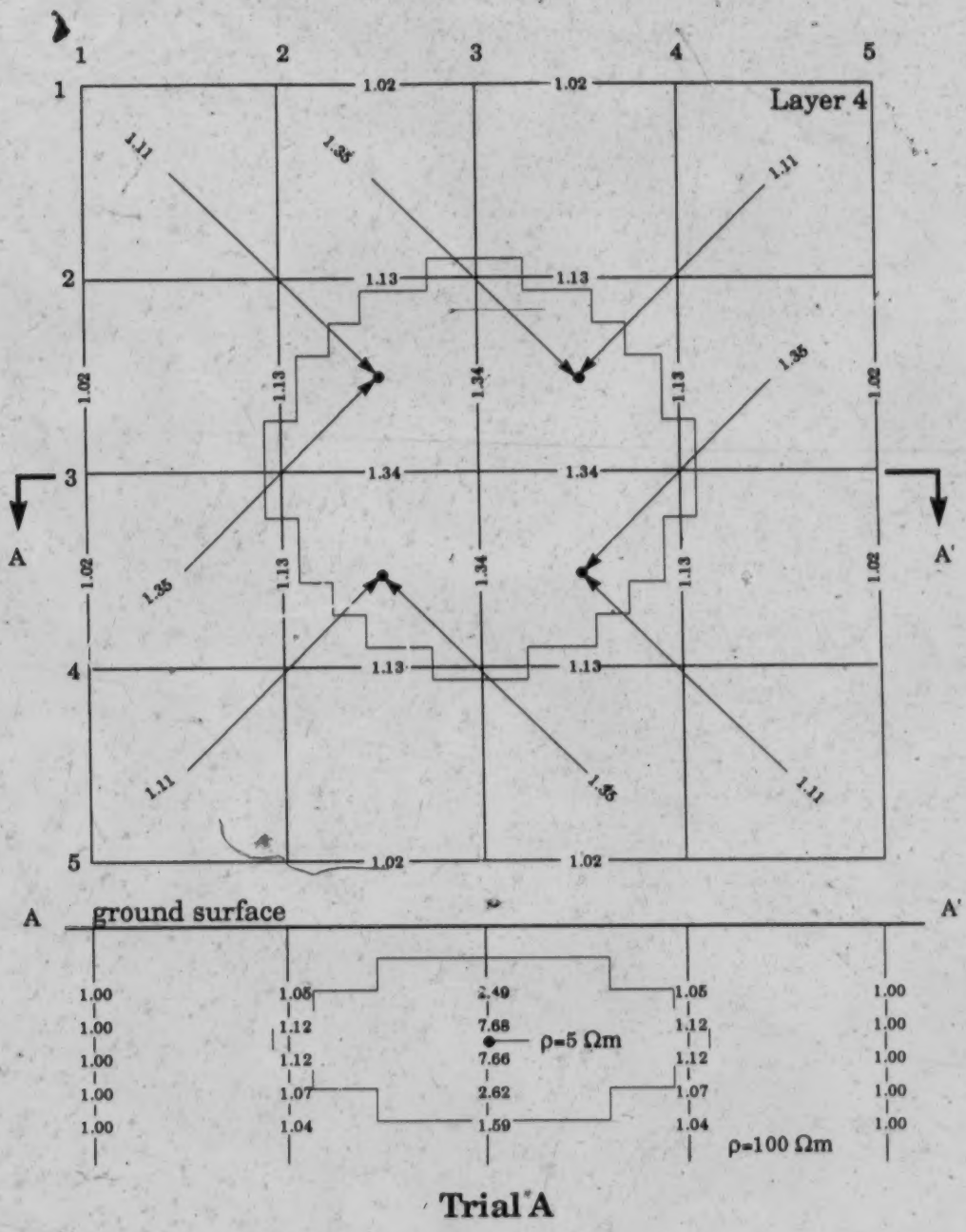

Figure 14. Selected downhole and crosshole scan results from Trial A.

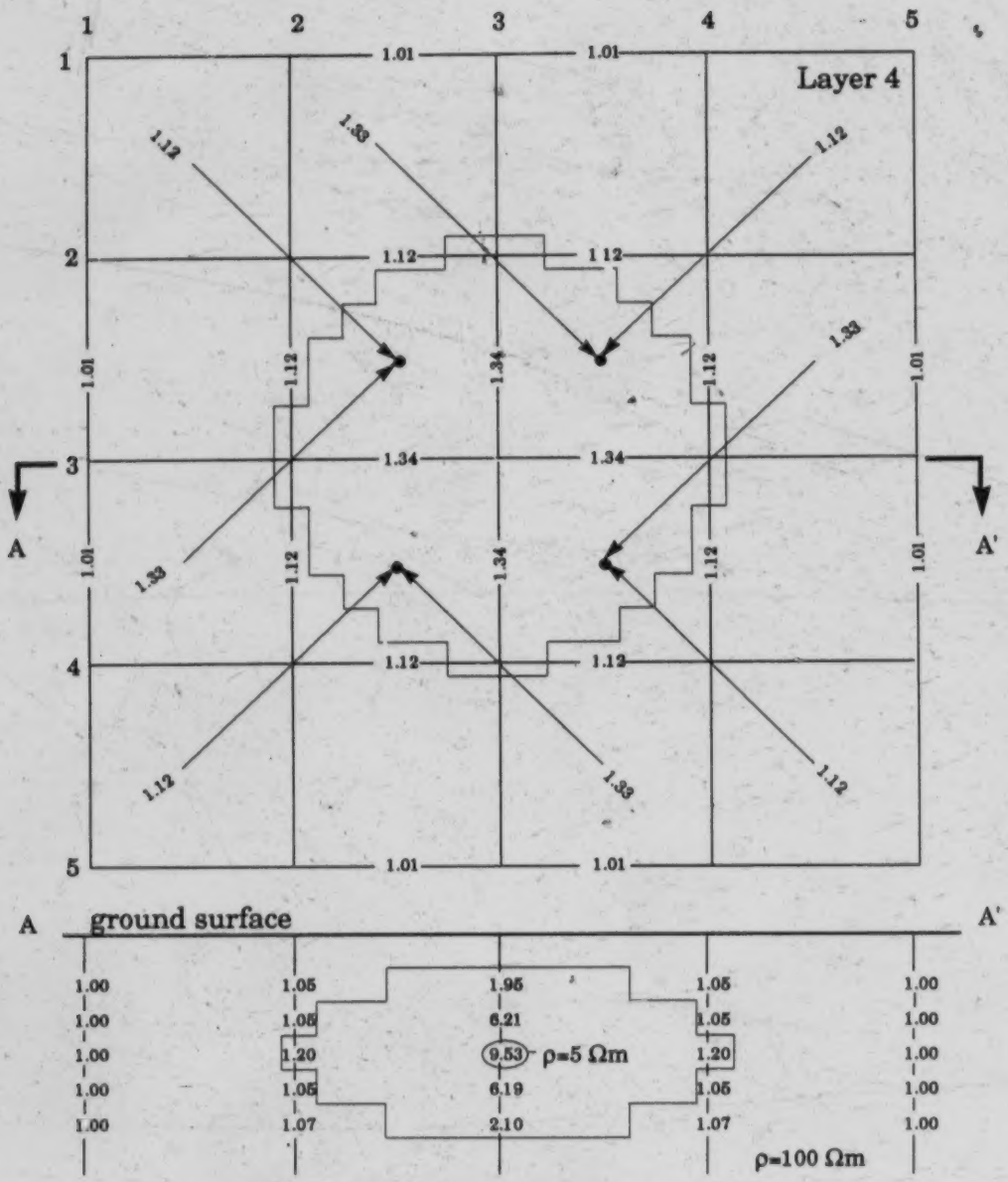

Trial B

Figure 15. Selected downhole and crosshole scan results from Trial B.

predicted aCR about the horizontal central plane of the anomaly. When the central plane coincides with the middle of two potential nodes (Trial B) then the predicted aCR is maximized at this location. Values above and below the plane fall off in response to decreasing conductivity. For the reference simulation, maximum values occur on either side of the central plane as it is now situated on a potential node. In all cases, the predicted results for the anomaly are less than the actual CR because of an averaging effect of the conductivity comprising the space around the current and potential nodes. For this particular anomaly, the predicted aCR at best (Trial B) underestimates the actual conductivity by about half.

With regard to the crosshole scan results, horizontal symmetry for both trials is now with respect to the vertical axis of the anomaly. However, the predicted aCR's are considerably smaller, relative to the downhole scans, owing to the larger "a" spacing and thus the more pronounced averaging of the conductivity about the current excitation volume. A comparison of the crosshole results from these two trials also shows how a subtle change in the vertical position of the anomaly has little bearing on the predicted aCR. There is, in fact, no significant difference between these results. As Table 5 shows, successive results from the layers above and below the central plane are also only subdued replicas of that obtained along the central plane itself.

Table 5 can also be used to compare the difference between a scan using this electrical method and that obtained by a conventional surface array. Although technically the results from layer 1 correspond to current being introduced one meter below the ground surface, for the

TABLE 5. Selected Crosshole Scan Results from Trial B

	Orthogonal Scan		Diagonal Scan	
	Electrode		Electrode	
Layer	2:3,3	2:3,4	2:3,3:4	2:3,2:3
1	1.09	1.09	1.19	1.14
2	1.10	1.10	1.22	1.15
3	1.34	1.12	1.27	1.14
4	1.34	1.12	1.33	1.12
5	1.30	1.12	1.32	1.10
6	1.25	1.10	1.26	1.09
7	1.21	1.09	1.19	1.09
8	1.17	1.07	1.14	1.08

purposes of this comparison they could be treated as the same as those results obtained along the ground surface. Relative to layer 4, which closely corresponds to the location of the horizontal central plane of the anomaly, the orthogonal scan and diagonal side scan results from layer 1 at electrodes 2:3,3 and 2:3,2:3 are lower by about 20% and 10%, respectively. If the horizontal central plane of the anomaly were moved down a few more layers then the surface method would not likely detect the anomaly at either of these "a" spacings, nor would the outcome improve with an expanded array.

The results obtained by the electrical method proposed here are not particularly high when operating in a crosshole manner. However, by introducing current and measuring voltages within the ground this technique provides better results than the surface method.

For trial C, the repositioning of the vertical axis between the four surrounding electrodes (see Figure 16) leads to the situation where most of the aCR information within the anomaly is collected from its sides. Hence, for the downhole scans, the predicted aCR values are still symmetric about the horizontal central plane but small as compared to the reference simulation. The four orthogonal and two diagonal scans of the anomaly provide slightly better results than trial A because both potential nodes are located closer to the vertical axis. However, even the predicted aCR, which straddles the vertical axis of the anomaly on the diagonal, is only about 10% of the actual conductivity. Interestingly enough, all of the closest downhole and crosshole scan results (both orthogonal and diagonal) to the centroid of the anomaly have about the same aCR (-1.9) despite differences in

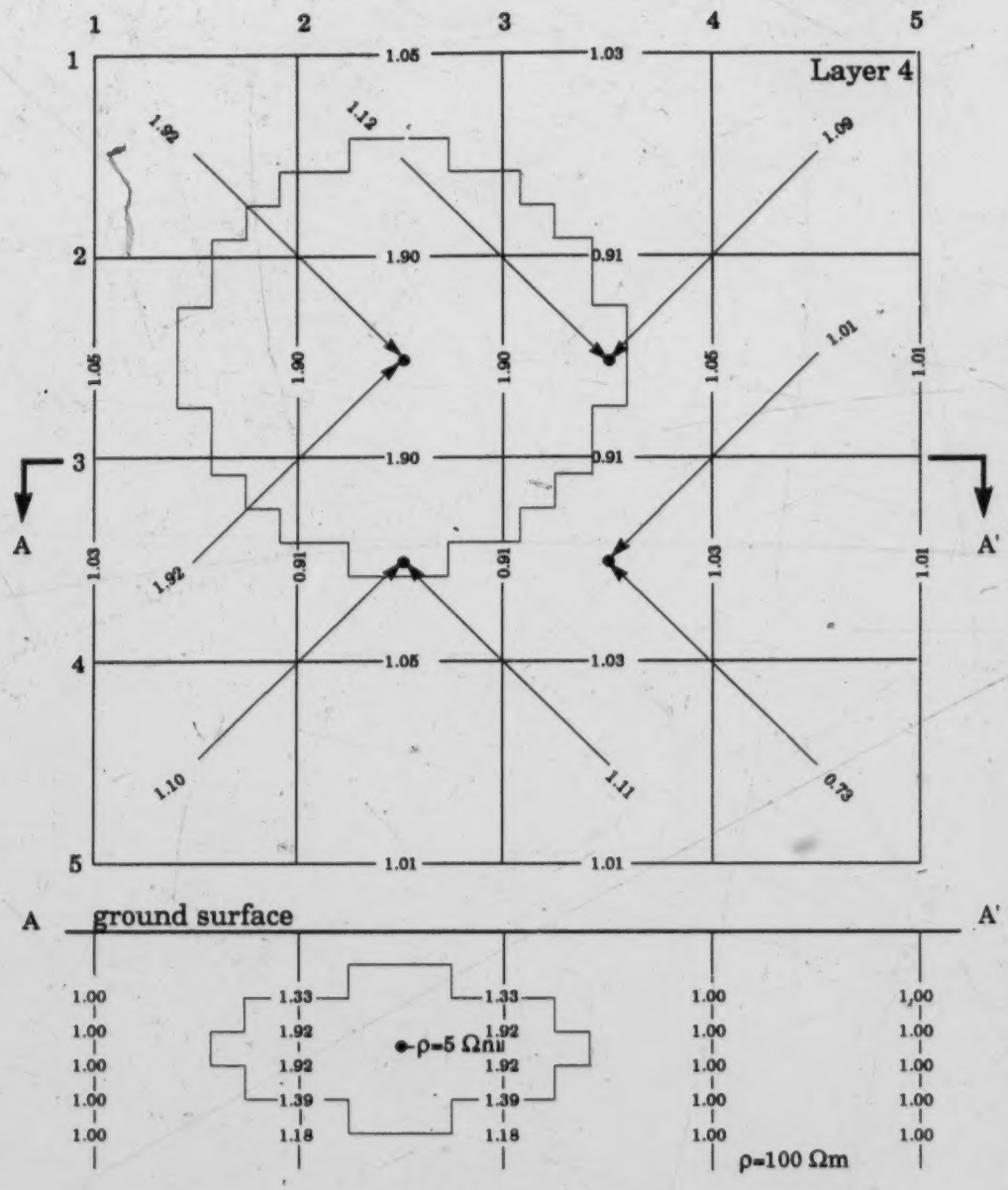

Trial C

Figure 16. Selected downhole and crosshole scan results from Trial C.

the "a" spacings. One aspect of Trial C not previously seen is the occurrence of an occasional undershoot in the aCR, i.e. a value less than 1.0. The implication is that a more resistive body lies within the medium. In actual fact this feature is simply an undesirable characteristic of apparent conductivity profiling. Undershoots usually occur when:

(1) the boundary between the anomaly and medium is normal or slightly skewed to the scanning direction.

(2) a large conductivity contrast is present between one current-potential nodal pair and the other, with the boundary between the anomaly and the medium located somewhere between the midpoint of the array and the potential node on the side of the anomaly.

Fortunately, undershoots usually stand out as singularities in the scan results. In conjunction with the entire aCR pattern they can be used to assist in determining the position of a boundary between an anomaly and the medium.

In a simulation in which the anomaly is simply positioned half a layer below that used for Trial C, the results (not shown) are as expected from the other simulations to this point. The aCR results from the downhole scan showed a slight improvement over that obtained from Trial C, owing to the fact the horizontal central plane of the anomaly was situated between two potential nodes. No significant difference existed between the crosshole scan results.

In summary, crosshole scans are not particularly useful in resolving the vertical position of an anomaly but rather its horizontal position as given by the predicted aCR pattern. Downhole scans can more accurately determine the vertical position of an anomaly, limit its probable horizontal extent and, because of its smaller "a" spacing, provide a closer estimate of the actual conductivity.

Size and Shape of Anomaly

Previous trials have shown how an apparent conductivity distribution can be used to infer the location of an anomaly based on systematic downhole and crosshole scans. These simulations involved an anomaly whose overall dimensions exceeded the nodal separation of the grid network. Hence, irrespective of position, some information would always be guaranteed with this particular anomaly. To evaluate the performance of the monitoring network using anomalies with different sizes and shapes, three trials (Trials D, E and F) were devised.

First, the effect of different ellipsoidal anomalies (S3 to S6) is considered (see Table 2 for summary details). Table 6 lists the anomaly types corresponding to each of these trials. Figure 17 illustrates the results from the downhole scans of these anomalies across layers 4:5 while Figure 18 provides the crosshole scan aCR's within layer 4. For ease in comparison, anomaly S4 (Trial A) is repeated on these two diagrams. All other parameters used for the reference case remain the same.

TABLE 6. Trials Where Anomalies with Different Sizes and Shapes are Varied

	Trial			
Parameter	A	D	E	F
anomaly type	S4	S3	S5	S6
location of centroid of above anomalies with respect to operational grid				
- x_o, y_o	3,3			
- z_o	4			

	Trial		
Parameter	C	G	H
anomaly type	S4	S3	S5
location of centroid of above anomalies with respect to operational grid			
- x_o, y_o	2:3,2:3		
- z_o	4		

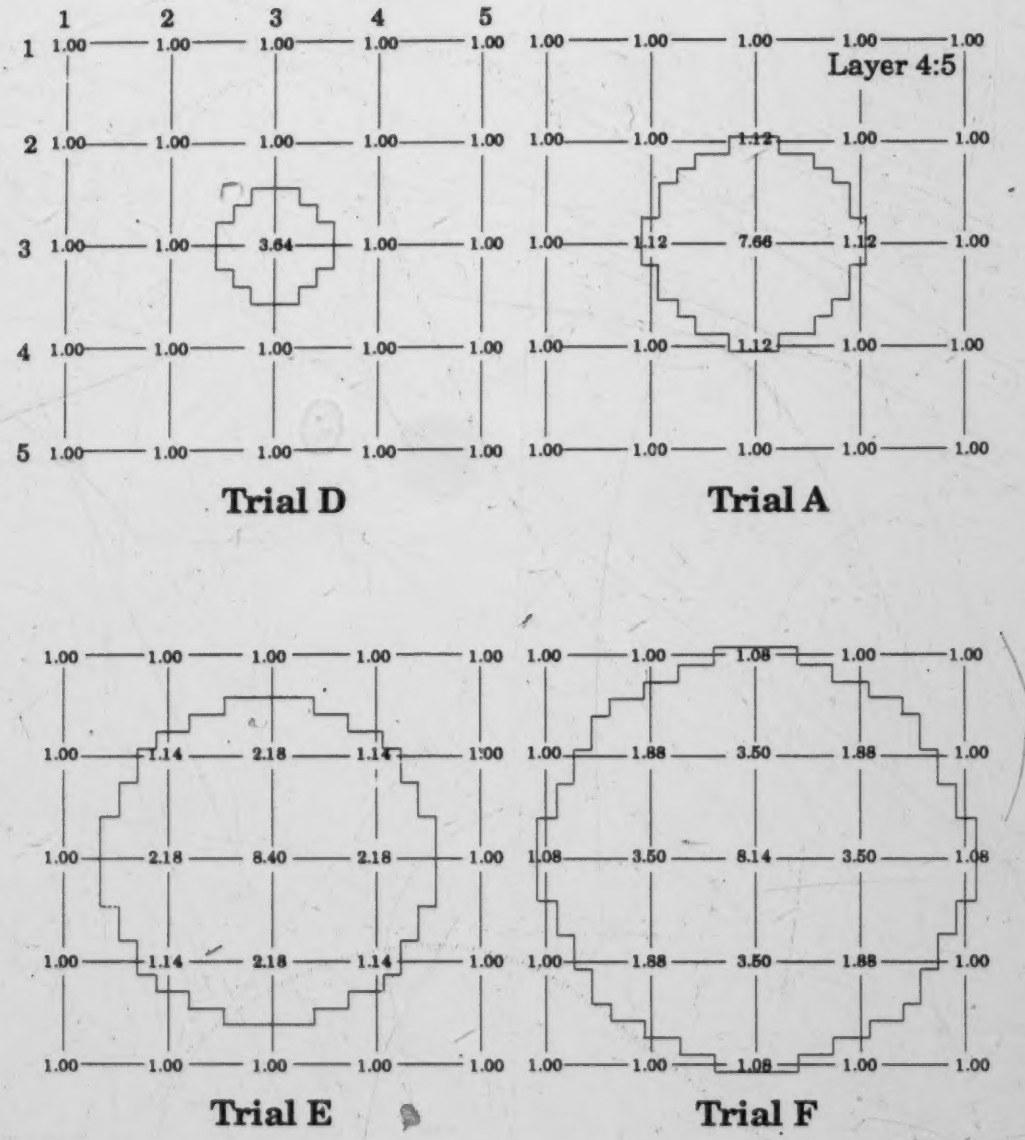

Figure 17. Selected downhole scan results from Trials A, D, E and F.

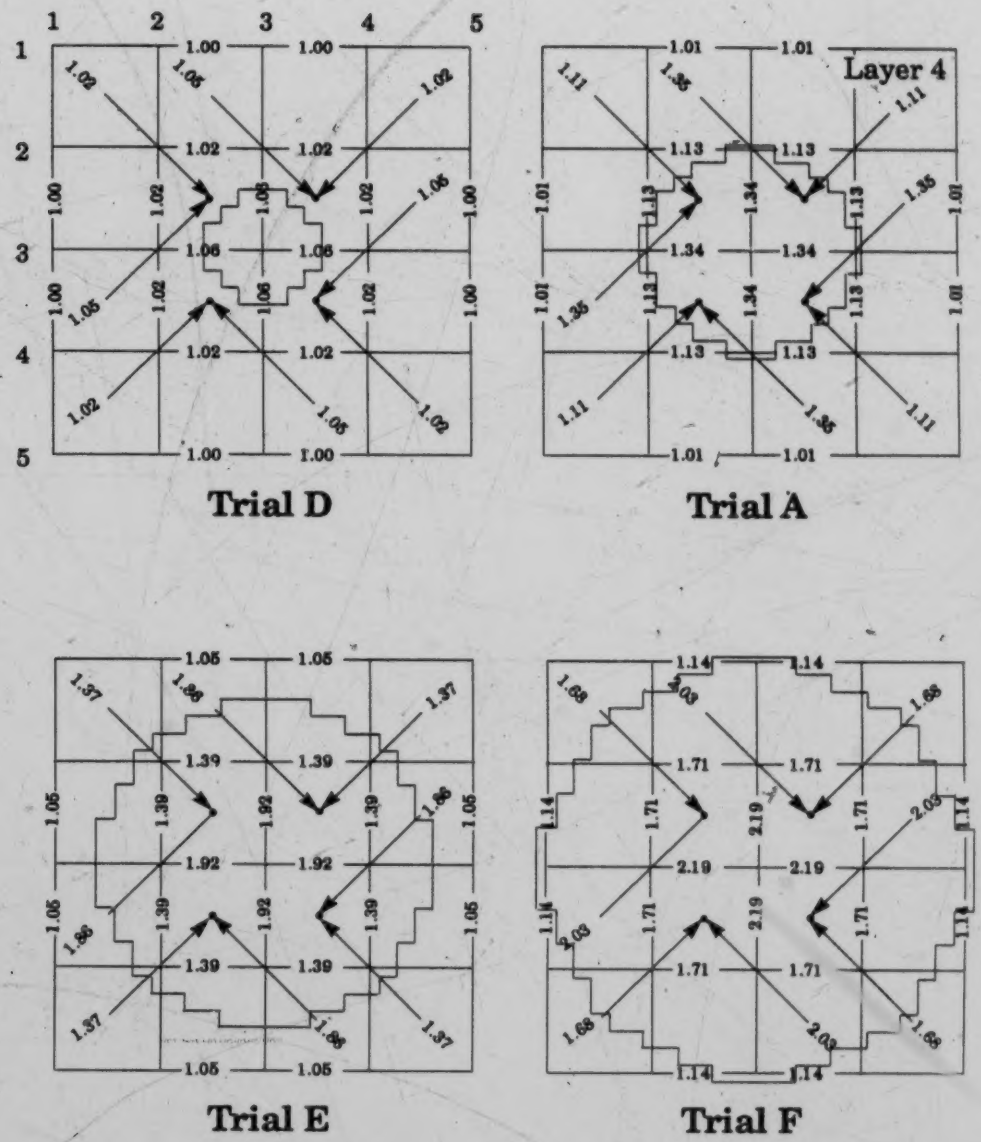

Figure 18. Selected crosshole scan results from Trials A, D, E and F.

A comparison of the downhole scans (Figure 17) clearly shows that given a sufficiently large anomaly relative to the grid network, the horizontal position can be determined even without the crosshole information. These scans also show the overall increase in the aCR values with larger anomalies. Refer to Table 7 for the results of the downhole scan from electrodes 2,3 and 3,3. The average of the actual CR corresponding with these results (layers 4 and 5) is shown for comparison. Differences in the aCR's largely reflect changes in the number of anomaly layers and the conductivity contrast between the anomaly and the medium (if any) at these points. At electrode 3,3 note how the aCR is not only sensitive to an increase in the number of anomaly layers, but also to changes in the actual CR. The results from both electrodes also show how the overall predicted aCR diminishes slightly in value relative to increases in the actual CR.

As might be expected, the crosshole scan results (Figure 18) also show an increase in value with larger anomalies but they are more subdued than the downhole aCR data as a consequence of the larger "a" spacing. The horizontal position of each anomaly is evident from the aCR pattern although, as was the case for example (a) in the preliminary trials, it is questionable whether Trial D would actually be detected. One salient point regarding a diagonal scan of an anomaly centered about an electrode is that when the scanning direction is normal to the boundary, comparable aCR values occur with the neighboring orthogonal results behind it. Similarly, a diagonal side scan of the anomaly produces results comparable to the neighboring orthogonal values closer to the enter of the anomaly. This was also evident for

TABLE 7. Selected Downhole Scan Results from Trials A,D,E and F

Anomaly	Trial	Number of Anomaly Layers at Electrode	Average of Actual CR	Predicted aCR
			Electrode 3,3	
S3	D	3	12.00	3.64
S4	A	5	15.05	7.66
S5	E	5	15.25	8.40
S6	F	5	14.85	8.14
			Electrode 2,3	
S3	D	0	1.00	1.00
S4	A	1	1.10	1.12
S5	E	3	2.95	2.18
S6	F	5	5.50	3.50

example (c) from the preliminary simulations. This occurs regardless of the size of the anomaly although a slight discrepancy between the comparable diagonal and neighboring orthogonal values becomes more pronounced with the larger anomalies.

Two further simulations (Trials G and H) involved placing anomalies S3 and S5 between four surrounding borehole electrodes. Anomaly S6 could not be positioned in this location because its dimensions would have exceeded the limits of the operational grid. The downhole and crosshole scan results are illustrated in Figures 19 and 20, respectively, while a summary of the anomaly types corresponding to these trials is given in Table 6. Trial C, which corresponds to the reference case in this position, is repeated on these diagrams for comparative purposes. For the downhole scans, the primary effect is that anomalies can be detected if their overall dimensions exceed the horizontal nodal spacing of the operational grid. As well, some inference can be made regarding their horizontal position. Unless a portion of the anomaly passes through the electrode, however, the downhole scan will not detect it. For the crosshole scans, two important points come to light. First, the presence of undershoots in the aCR's can be used to confirm the position of an anomaly's boundary, noting it is approximately situated between one of the two current-potential electrode pairs. Second, for this particular situation, the point corresponding to the two highest diagonal scan results is also the location of the central axis of the anomaly if these two diagonal aCR's and the four surrounding orthogonal results are all equal in value.

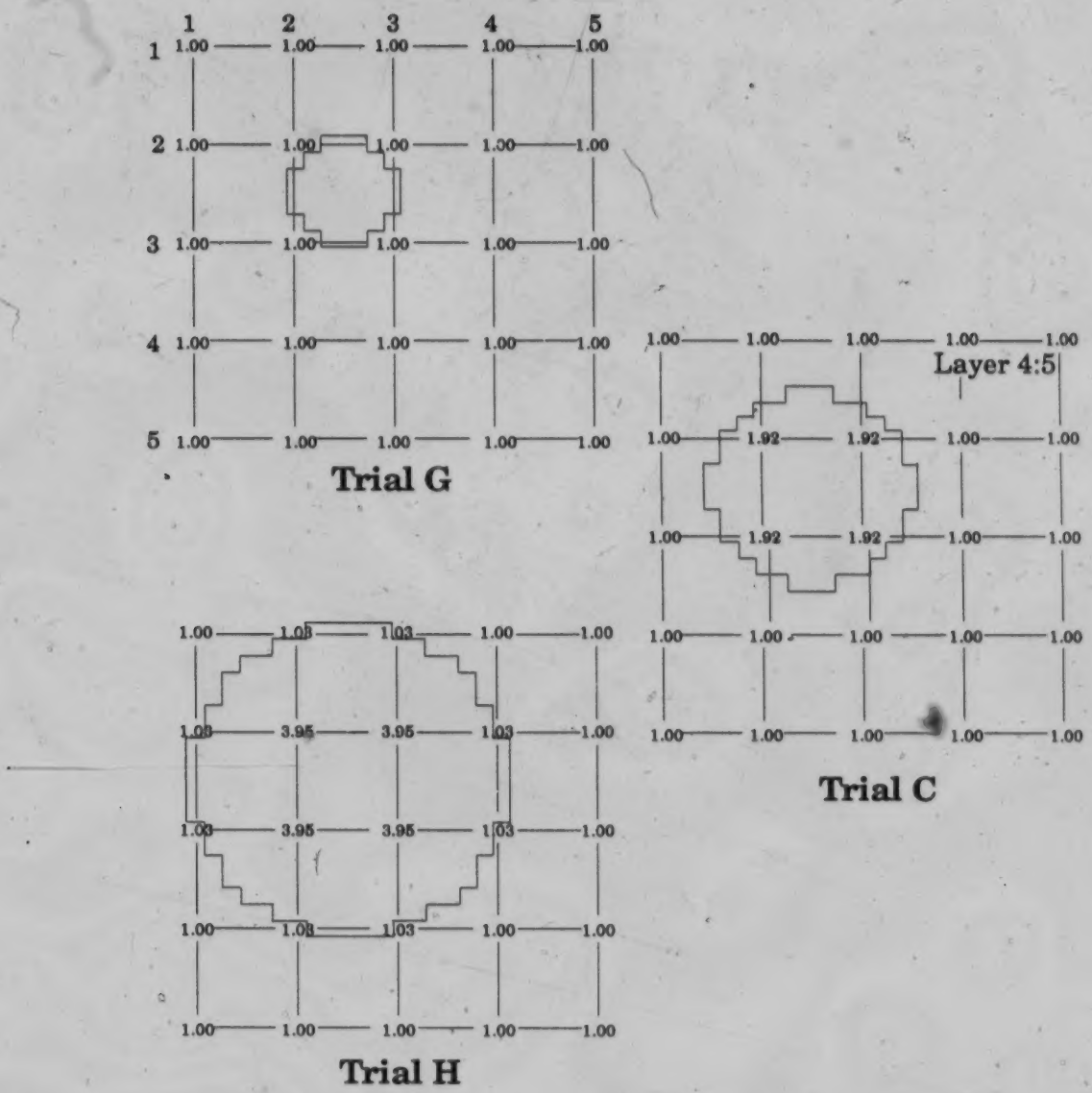

Figure 19. Selected downhole scan results from Trials C, G and H.

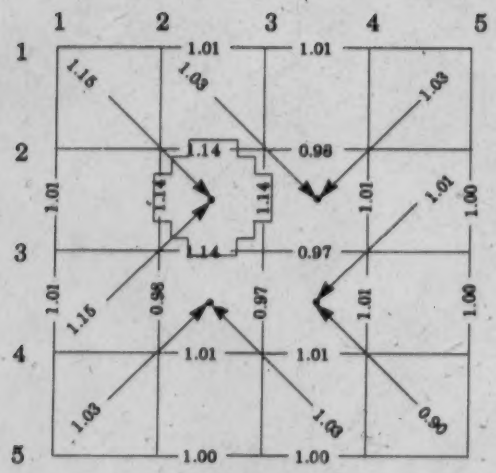

Trial G

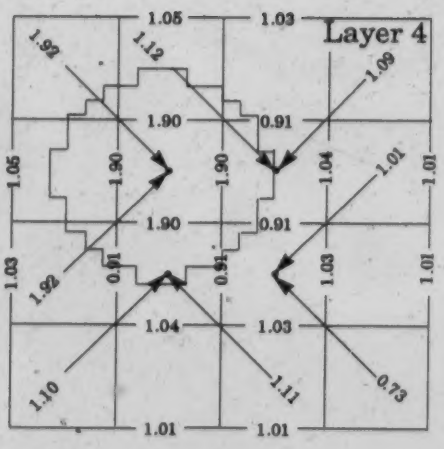

Trial C

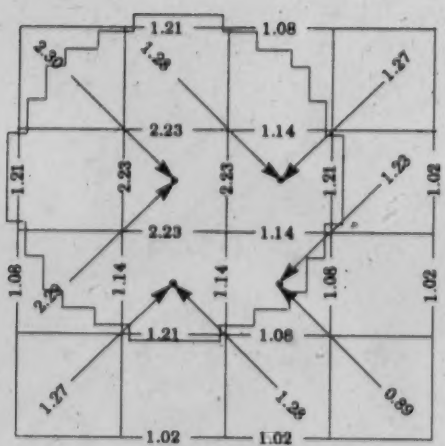

Trial H

Figure 20. Selected crosshole scan results from Trials C, G and H.

The effect of the size and shape of the two smaller, spherical anomalies (S1 and S2) was also examined. Simulations carried out (not shown) with anomaly S1 indicated that the only situation in which it could be detected was when it was virtually positioned at an electrode and then only by a downhole scan. It was not possible to detect this small an anomaly with a crosshole scan under any circumstances, or by a downhole scan once it was horizontally repositioned more than one node away from an electrode. Similarly, anomaly S2 could only be detected by a downhole scan if it was positioned at, or very close to, an electrode. It was not significantly detected by a crosshole scan under any condition. Note also that the conclusions which are drawn for both of these anomalies involve uniform internal conductivity distributions since they are too small for a gradational distribution.

In summary, for an anomaly to be detected by a downhole scan it must be positioned such that the scan will pass through a portion of the anomaly. This at the very least will enable the vertical position to be determined. The overall size and shape of the anomaly relative to the operational grid will dictate the degree of interpretation which can be made regarding its horizontal position by downhole and/or crosshole scans.

Non-Uniform Medium

In all of the simulations carried out to this point, anomalies were analyzed within a medium containing uniform properties. This was treated as a fully saturated medium composed of clean sands. For each

scenario, residual apparent conductivity distributions were obtained by dividing the voltage from each scan by its respective background voltage; all other parameters involving the electrode array being equal. This procedure, in effect, simply normalized the output. In this section, the influence of a heterogeneous medium on the apparent conductivity pattern is considered.

The effect of a medium with an unsaturated zone is first examined. In Trials I and J, three additional layers are added to the top of the overall grid. Trial I involves placing a zone of unsaturated clay in these layers, while in Trial J, a zone of unsaturated clean sand is used. These two trials could also be viewed as a simple case involving a zone containing the same soil type but different in its soil moisture or temperature conditions. Equivalent resistivities assigned to these two zones are 200 ohm-m and 500 ohm-m, respectively. Apart from the addition of the three layers to the grid, all other parameters used for the reference case remain the same. Table 8 is a summary of the above. The output is presented in two different ways. One involves presenting the apparent resistivity distribution as predicted, while the other is the normalized conductivity version. The first way of looking at the results highlights the influence of each layered heterogeneity on the predicted results. The second shows how the residual apparent conductivity approach enables the same solution to be obtained, irrespective of the presence of a heterogeneity. As a result of adding three layers to the grid, crosshole scans could not be simulated because the dimensions of this grid exceeded the storage capabilities of the computer.

TABLE 8. Trials Where Additional Layers are Added to the Medium Representing Zones of Higher Resistivity

Parameter	Trial A	Trial I	Trial J
resistivity of unsaturated zone, ohm-m (layers 1 - 3)	n/a	200	500
resistivity of saturated zone, ohm-m (layers 4 - 11)	100	100	100

A comparison of the downhole predicted apparent resistivities for the reference case and Trials I and J is shown in Figure 21. Relative to the reference case, the main effect to note is the downward influence of the more resistive unsaturated zone about two layers below the interface with the saturated zone. In Trials I and J there is an apparent resistivity increase in the results immediately below the interface due to the presence of the unsaturated zones. As they stand, interpretation of these distributions is not particularly difficult but it does require consideration of the near surface soil type and/or moisture and temperature conditions.

Compare this result with the normalized version of this same data set (Figure 22). By taking into account the prevailing background conditions, the effect of normalizing the data is to still obtain the same results as the reference case, even if the background conditions are non-uniform either in space (soil type) or over time (moisture-temperature conditions). The three aCR distributions are virtually identical. The overall result is to accentuate the presence of the anomaly as opposed to other factors which could influence the aCR pattern.

To examine the effect of a heterogeneity beside the anomaly one last trial (Trial K) was carried out in which a conductive clay lens was positioned beside the anomaly used for the reference case. The results from this trial were normalized in two ways. One was by using the correct background conditions, i.e. taking into account the effect of the clay lens. The other was by deliberately using an arbitrary

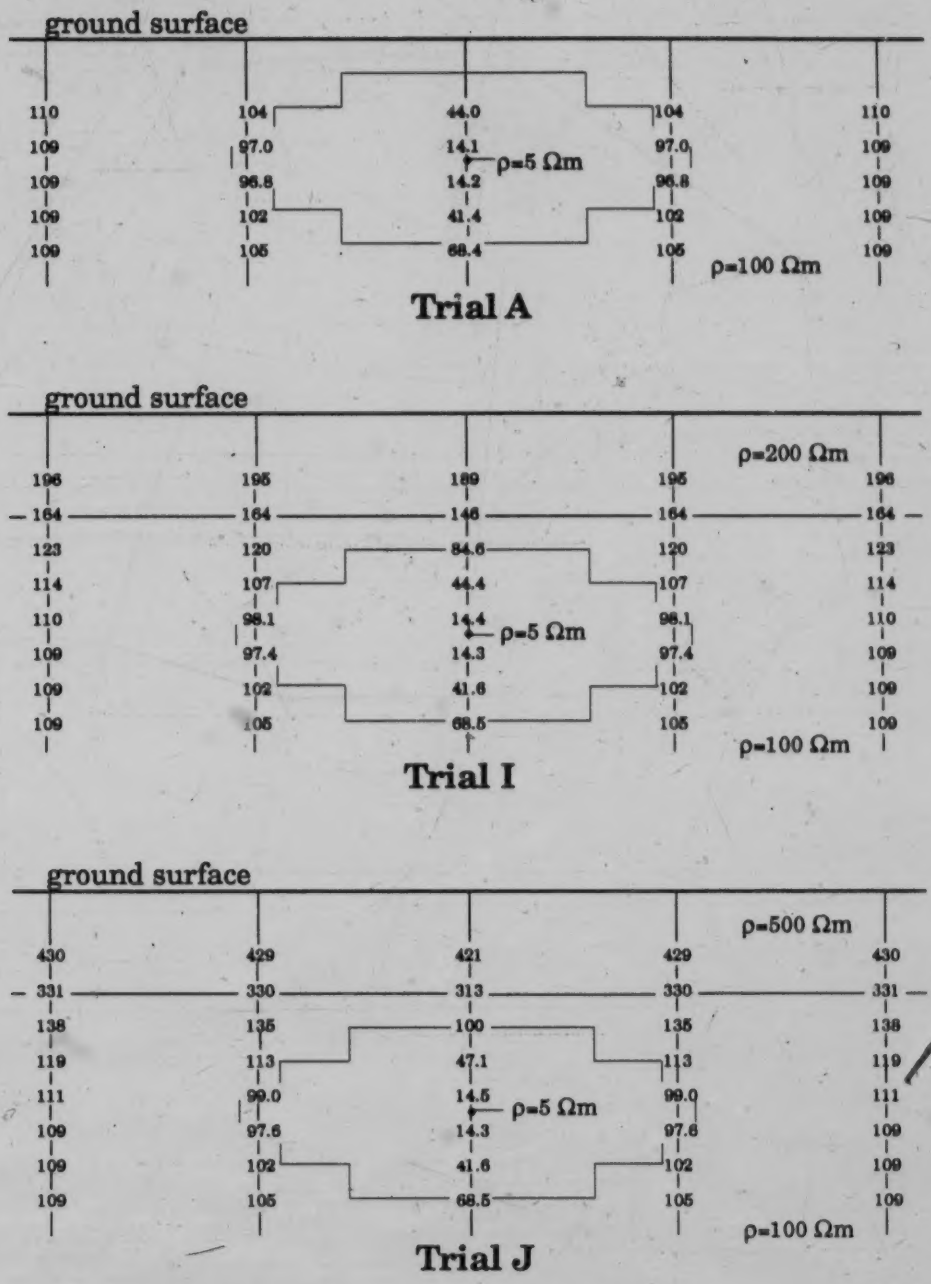

Figure 21. Selected downhole scan results from Trials A, I and J showing the apparent resistivity.

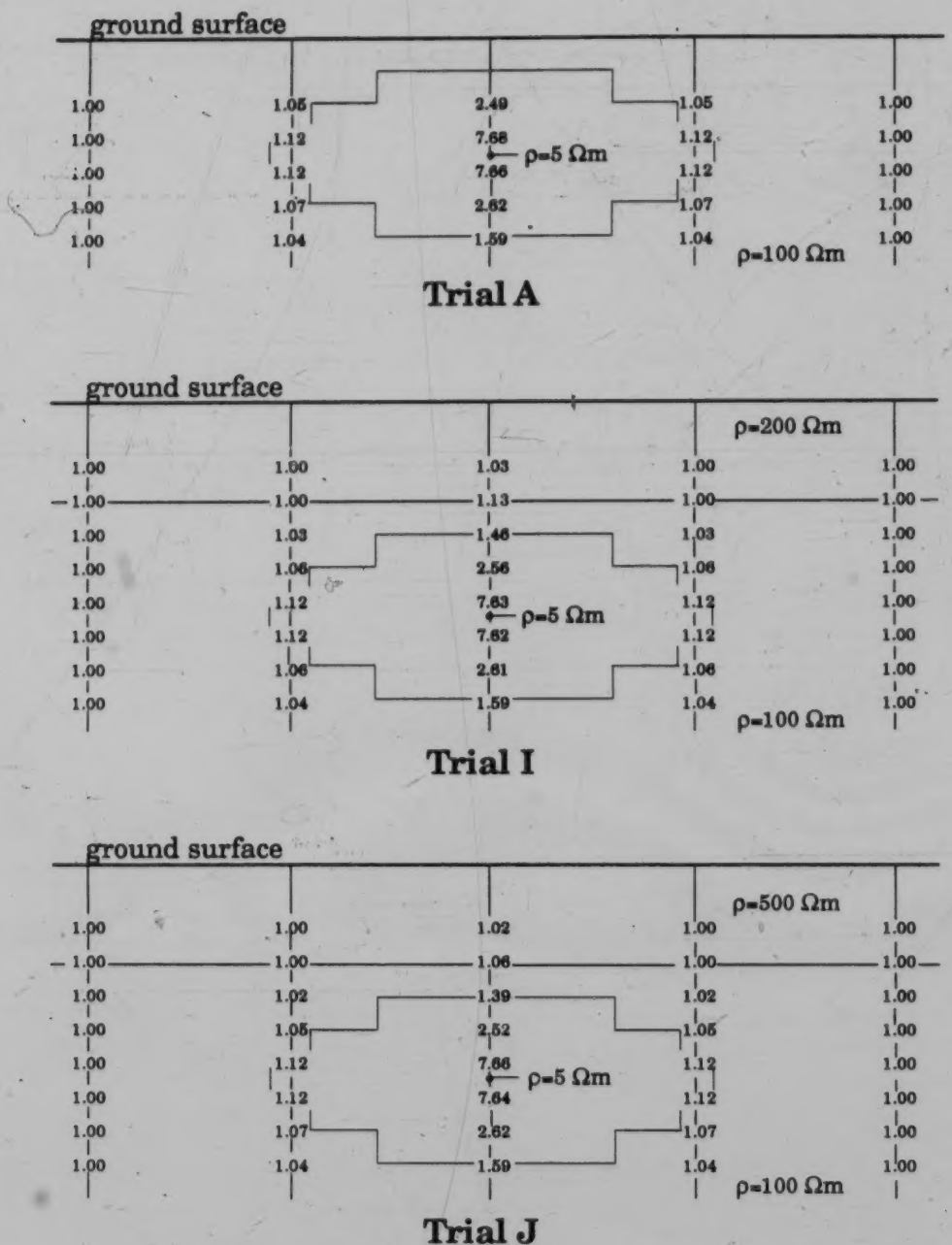

Figure 22. Selected downhole scan results from Trials A, I and J showing the aCR corrected with the prevailing background conditions.

background consisting of a uniform medium. This was done in order to demonstrate how an incorrect interpretation of the aCR pattern could be made if heterogeneities in the medium are not recognized. As before, other parameters are identical to that used for the reference case. The results using a uniform background which does not account for the presence of the clay lens are depicted in Figure 23. This arbitrary use of a singular value to be used as the background condition is a common practice in exploratory application of the electrical method. Since pre-contamination conditions are not known "a priori", a background value is selected from an off-site area similar in characteristics. In this case both the downhole and crosshole scans have detected its presence, but the interpretation of the crosshole pattern is confusing due to undershoots in the output data.

Compare this now to Figure 24 where use of the correct background conditions has eliminated the influence of the clay lens on the results. This leads to clearer picture of the subsurface conditions. The correct version of the results from Trial K are the same as that obtained from Trial A (see Figure 14).

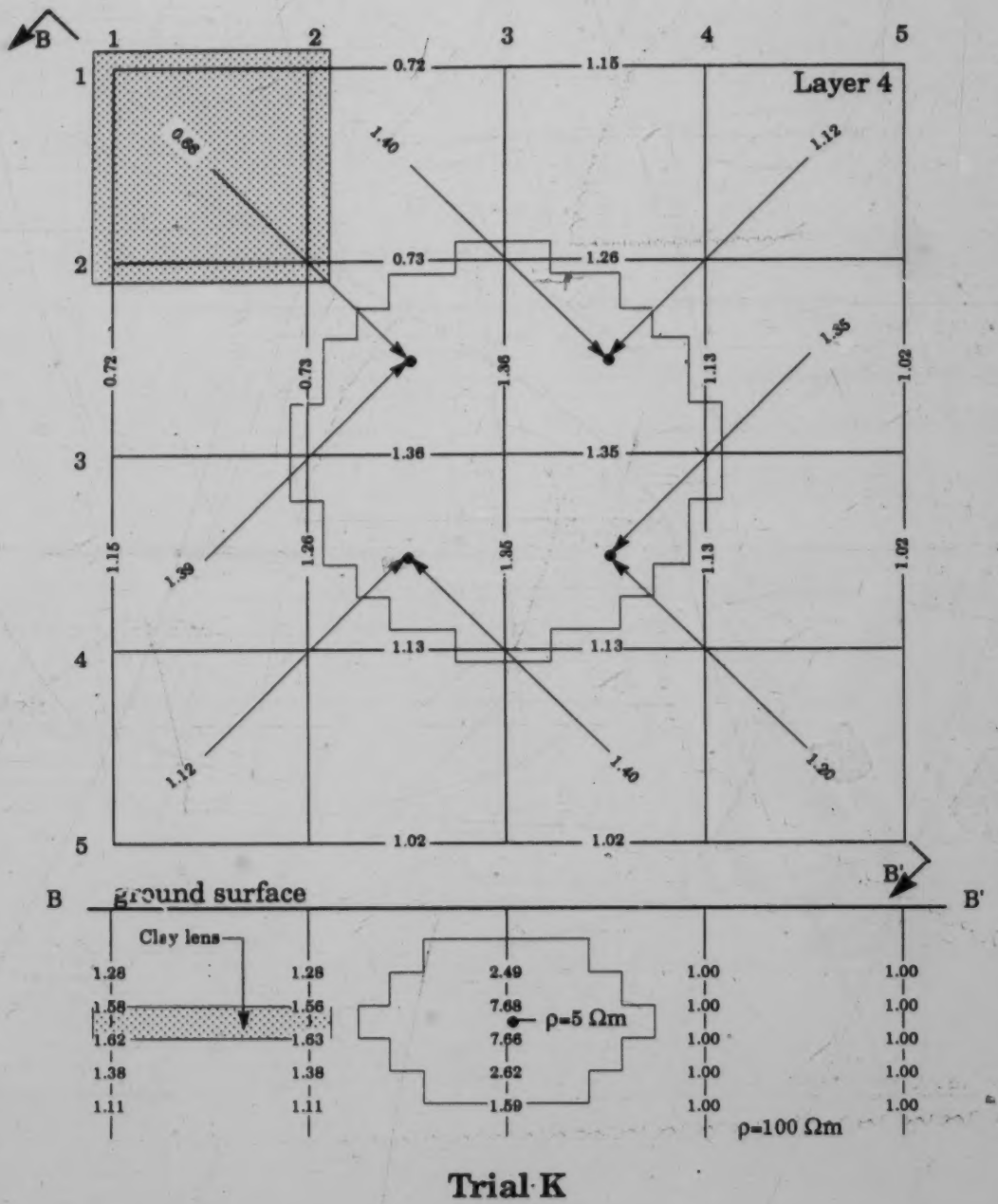

Trial K

Figure 23. Selected downhole and crosshole scan results from Trial K showing the effect of an incorrect use of the background conditions.

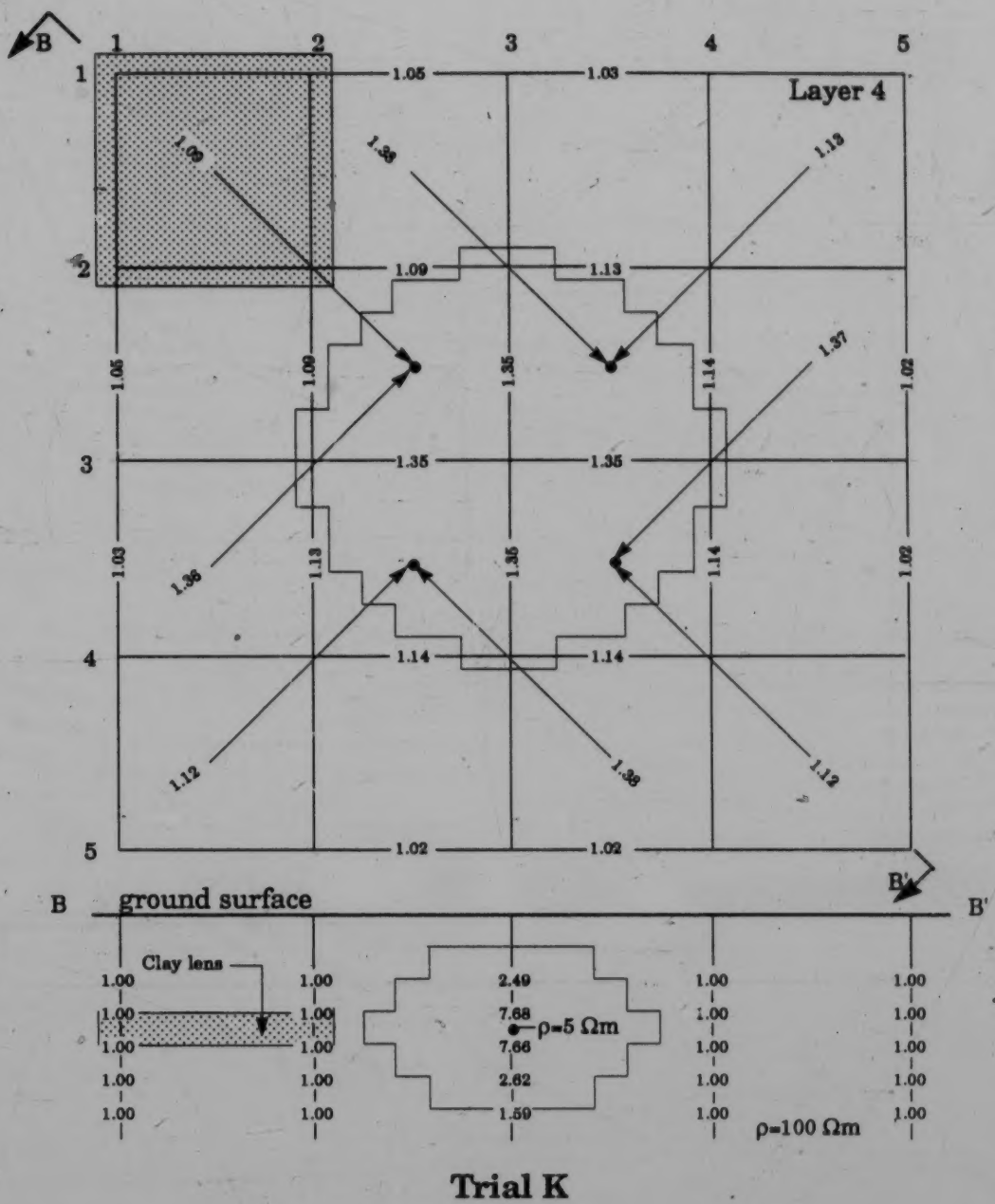

Trial K

Figure 24. Selected downhole and crosshole scan results from Trial K corrected with the prevailing background conditions. Compare these results to those shown for Trial A (Figure 14).

5. CONCLUSIONS

1. These simulations show that contaminants introduced into the ground can be more accurately monitored by a borehole electrical method using a three-dimensional grid of electrodes. This approach has the potential of more accurately resolving contaminant distributions than a conventional surface electrical technique. This is expected because current is not only introduced directly into the subsurface but also because all voltage measurements are made below ground. This technique provides for a more focused and systematic investigation of the region covered by the grid, and avoids the loss of information with depth. This problem inevitably accompanies the surface method because of the associated increase in the "a" spacing.

2. The factors which influence the ability of the borehole electrical method to detect an anomaly (given a sufficient conductivity contrast with a medium) are the size, shape and position of the anomaly relative to the grid spacing. The downhole scan is more effective in determining the vertical position of an anomaly and, depending on the extent of an anomaly, may be able to assist in fixing its horizontal location. For this to occur, however, the anomaly must be positioned at or very close to an electrode such that a downhole scan passes through it. Providing the horizontal extent of an anomaly is roughly equal to, or exceeds, the horizontal spacing between electrodes, crosshole scans can be used

to infer the horizontal position of an anomaly. Because of the narrower "a" spacing used for downhole scans, they provide a better estimate of the actual conductivity than crosshole scans. However, it is the symmetry or asymmetry of the apparent conductivity pattern which is used to infer the position of an anomaly relative to the grid network.

3. Other factors which affect the apparent conductivity distribution are those which lead to a non-uniform medium such as different soil types, moisture content, temperature or perhaps a temporal change in the latter two. The residual conductivity approach enables these influences to be eliminated providing that:

   (a) disruption of the region immediately encompassing the grid does not occur.

   (b) the correct set of background readings, appropriate for the governing conditions at the time of use, are selected from a seasonal suite of data.

4. It is clear that an inground electrical method could not itself meet the ideal demands of a monitoring network; i.e. provide an accurate yet cost-effective means of detecting and delineating a contaminant plume. However, in combination with chemical data obtained from wells, it is suggested that the two systems would complement each other very well in fulfiling these requirements. Data from wells could be used to occasionally provide accurate

information concerning the presence and distribution of specific chemical species. The electrical method, on the other hand, could assume the routine low-cost detection duties and provide an outline of the general extent of any plume that may form.

5. The results from this theoretical examination of the inground electrical method suggest that further research is warranted using experimental data. Validation of a concept is a logical next step. This work would involve physical modeling using either a sand tank or an actual field site. In addition, this study would help to assess the importance of other factors which are known to influence electrical conductance in the subsurface, and to provide practical experience for the design and operation of the network.

REFERENCES

Cartwright, K. and M. R. McComas, Geophysical Surveys in the Vicinity of Sanitary Landfills in Northeastern Illinois, Ground Water, 6(5), 23-30, 1968.

Daniels, J.J., Three-Dimensional Resistivity and Induced-Polarization Modeling Using Buried Electrodes, Geophysics, 42(5), 1006-1019, 1977.

Dey, A. and H.F. Morrison, Resistivity Modeling for Arbitrarily Shaped Three-Dimensional Structures, Geophysics, 44(4), 753-780, 1979.

Hackbarth, D.A., Field Study of Subsurface Spent Sulfite Liquor Movement Using Earth Resistivity Measurements, Ground Water, 9(3), 11-16, 1971.

Jakosky, J.J., Exploration Geophysics, Trija Publishing Co., Los Angeles, 1950.

Karplus, W.J., Analog Simulation; Solution of Field Problems, McGraw-Hill, New York, 1958.

Keller, G.V. and F.C. Frischknecht, Electrical Methods in Geophysical Prospecting, Pergamon Press, Toronto, 1966.

Klefstad, G., L.V.A. Sendlein and R.C. Palmquist, Limitations of the Electrical Resistivity Method in Landfill Investigations, Ground Water, 13(5), 418-427, 1975.

Kunetz, G., Principals of Direct Current Resistivity Prospecting, (tr. by Van Nostrand, R.) Gebruder Borntraeger, Verlagsbuchhandlung, Berlin-Nikolassee, 1966.

McDonald, M.G. and A.W. Harbaugh, A Modular Three-Dimensional Finite-Difference Ground-Water Flow Model, U.S.G.S., Reston, 1985.

McNeil, J.D., Electrical Conductivity of Soils and Rocks, Technical Note TN-5, Geonics Limited, 1980.

Reed, P.C., K. Cartwright and D. Osby, Electrical Earth Resistivity Surveys near Brine Holding Ponds in Illinois, Illinois State Geological Survey, Environmental Geology Notes 95, 1981.

Rushton, K.R. and S.C. Redshaw, Seepage and Groundwater Flow, John Wiley & Sons, Chichester, 1979.

Tamburi, A., R. Allard and U. Roeper, Tomographic Imaging of Ground Water Pollution Plumes, in Proceedings Second Canadian/American Conference on Hydrogeology, Alberta Research Council/NWWA, 162-167, Banff, Alberta, 1985.

Wexler, A. and C.J. Mandel, An Impedance Computed Tomography Algorithm and System for Ground Water and Hazardous Waste Imaging, in Proceedings Second Canadian/American Conference on Hydrogeology, Alberta Research Council/NWWA, 156-161, Banff, Alberta, 1985.

Wilt, M.J. and C.F. Tsang, Monitoring of Subsurface Contaminants with Borehole/Surface Resistivity Measurements, NWWA Conference on Surface and Borehole Geophysical Methods in Ground Water Investigations, 167-177, Fort Worth, Texas, 1985.